HHS Public Access

Author manuscript

Pain. Author manuscript; available in PMC 2021 November 01.

Published in final edited form as:

Pain. 2020 November ; 161(11): 2551–2570. doi:10.1097/j.pain.0000000000001955.

A modulator of the low-voltage activated T-type calcium channel that reverses HIV glycoprotein 120-, paclitaxel-, and spinal nerve ligation-induced peripheral neuropathies

Song Cai[‡,¶], **Peter Tuohy**[†,¶], **Chunlong Ma**[†], **Naoya Kitamura**[†], **Kimberly Gomez**[‡], **Yuan Zhou**[‡], **Dongzhi Ran**[‡], **Shreya Sai Bellampalli**[‡,a], **Jie Yu**[‡], **Shizhen Luo**[‡], **Angie Dorame**[‡], **Nancy Yen Ngan Pham**[‡], **Gabriella Molnar**[‡], **John M. Streicher**[‡], **Marcel Patek**[¢], **Samantha Perez-Miller**[‡], **Aubin Moutal**[‡], **Jun Wang**[†,*], **Rajesh Khanna**[‡,#,¥,Δ,*]

[†]Department of Pharmacology and Toxicology, College of Pharmacy, The University of Arizona, Tucson, Arizona 85721, United States

[‡]Department of Pharmacology, College of Medicine, The University of Arizona, Tucson, Arizona, 85721, United States

[¢]Bright Rock Path Consulting LLC, Tucson, AZ

[#]BIO5 Institute, 1657 East Helen Street, P.O. Box 210240, Tucson, AZ 85721, United States

[¥]The Center for Innovation in Brain Sciences, The University of Arizona Health Sciences, Tucson, Arizona, United States

[Δ]Regulonix LLC, Tucson, Arizona, United States

Keywords

Low-voltage activated calcium channel; T-type; peripheral neuropathy; non-opioid; Ugi-azide four-component reaction

1. Introduction

Neuropathic pain is a major health burden [27]. Despite intense research on the topic, very limited non-opioid treatments are available as alternatives. A failure to develop new drugs to combat pain is primarily because neuropathic pain is a complicated disease that can originate from many different types of injuries (nerve injury, chemotherapy [70], human immunodeficiency virus -HIV- infection [1] and others) and whose establishment involves central and peripheral systems. While neuropathic pain is a multisystemic disease, spinal block has been clinically demonstrated to curb neuropathic pain in patients [32]. Thus,

[*]corresponding author: Rajesh Khanna, Tel: 520-626-4281, Fax: 520-626-2204, rkhanna@email.arizona.edu.
[a]Present address: Mayo Clinic School of Medicine, 26 Mayo Park Dr SE, Rochester, MN 55904 United States
[¶]These authors contributed equally

CONFLICT OF INTERESTS STATEMENT

R. Khanna is the co-founder of Regulonix LLC, a company developing non-opioids drugs for chronic pain. In addition, R. Khanna has patents US10287334 and US10441586 issued to Regulonix LLC. R. Khanna and Jun Wang have filed disclosures on the composition of matter and use of **5bk**. The other authors declare no competing financial interest.

targeting molecular components of spinal transmission is a valid therapeutic strategy for the treatment of chronic neuropathic pain [8] as evidenced by the N-type voltage gated calcium channel (CaV2.2) blocker Prialt® [82].

Ion channels regulating afferent fiber excitability and synaptic function in the spinal dorsal horn are prime targets for the treatment of neuropathic pain [81]. One of these channels is the T-type Ca^{2+} channel [9]. These voltage-gated ion channels have a half activation voltage of ~ –45 mV [78], thus their contribution to the initiation of an action potential precedes the contribution of Na^{+} channels. The family of T-type Ca^{2+} channels contain three isoforms in mammals, CaV3.1, CaV3.2 and CaV3.3 with distinct expression pattern in tissues [41; 43]. In dorsal root ganglia (DRG) neurons, the predominant CaV3 channel isoform involved in pain signaling is CaV3.2 [4; 6]. CaV3.2 expression is restricted to the nociceptive Aδ- and C- low-threshold mechanoreceptors (LTMRs)[22]. CaV3.2 expression is increased following nerve injury [26]. Cav3.2 activity is also increased in paclitaxel-induced peripheral neuropathy [21; 58; 65; 87]. A specific role of CaV3.2 in pain was demonstrated by the observation that silencing this channel in DRG neurons reversed neuropathic pain in rats while silencing CaV3.1 or CaV3.3 did not [6]. Further evidence in support of CaV3 channels as important therapeutic targets for pain comes from studies of the T-type Ca^{2+} channels inhibitors ethosuximide [13; 31; 69], mibefradil, TTA-A2 or TTA-P2 [14; 77] – all of which reverse experimental neuropathic pain in rodents. However, clinical trials using T-type Ca^{2+} channel blockers for pain, such as ABT-639 [77] and MK-8998 [19], failed to meet the expected clinical endpoints. This may have been due to lack of selectivity for CaV3.2 leading to dose limitations. Another promising compound that may advance to clinic is Z944 [42; 80], but this molecule targets all CaV3 isoforms and may have the same clinical limitations as its predecessors. Thus, there is a need for a specific CaV3.2 blocker. We have shown before that the natural compound betulinic acid preferentially targets CaV3.2, and could reverse allodynia in the paclitaxel induced peripheral neuropathy and HIV related sensory neuropathy models [3].

Here we report the discovery of a T-type calcium channel modulator (**5bk**) that reverses mechanical allodynia in experimental models of neuropathic pain. As **5bk** did not affect locomotion or anxiety and was without action on opioid receptors, it appears to be a promising, safe, non-opioid candidate for the treatment of neuropathic pain by virtue of its selective block of CaV3.2 channels.

2. Materials and Methods

An expanded version of all Methods is available in the Supplementary Information section.

2.1. Compound synthesis and characterization.

Compound synthesis and characterization can be found in the Supplementary Information section.

2.2 Animals.

Pathogen-free adult male and female Sprague-Dawley rats (225–250g; Envigo, Indianapolis, IN) were housed in temperature-controlled (23±3 ˚C) and light-controlled (12-h light/12-h

dark cycle; lights on 07:00–19:00) rooms with standard rodent chow and water available ad libitum. The Institutional Animal Care and Use Committee of the College of Medicine at the University of Arizona approved all experiments. All procedures were conducted in accordance with the Guide for Care and Use of Laboratory Animals published by the National Institutes of Health and the ethical guidelines of the International Association for the Study of Pain. Animals were randomly assigned to treatment or control groups for the behavioral experiments. Animals were initially housed 3 per cage but individually housed after the intrathecal cannulation. All behavioral experiments were performed by experimenters who were blinded to the experimental groups and treatments.

2.3. Preparation of acutely dissociated dorsal root ganglion neurons

Dorsal root ganglia from all levels were acutely dissociated using methods as described previously [23]. Rat DRG neurons were isolated from 100g female Sprague-Dawley rats using previously developed procedures [53].

2.4. Calcium imaging in acutely dissociated dorsal root ganglion neurons

Calcium imaging on DRG neurons was performed as described previously [3].

2.5. Dorsal root ganglia neuron transfection.

Collected cells were re-suspended in Nucleofector transfection reagent containing siRNA at 500 nM and 2 μg of the provided GFP plasmid as detailed previously [17]. The siRNA sequences used were: UAGAUAGCAAAUACUUUGGCCGGGG (for Cacna1g/CaV3.1; (Cat# RSS355855, Thermofisher)); CAGCCAUCUUCGUGGUGGAGAUGAU (for Cacna1h/CaV3.2; (Cat# RSS350286, Thermofisher)); CAGCAUCCUUGGGAUGCAUAUCUUU (for Cacna1i/CaV3.3; Cat# RSS367566); and siRNA Negative Control, Med GC was used as a scrambled siRNA control (Cat# 12935300). Cells were used 48 hrs after transfection.

2.6. Constellation Pharmacology.

These experiments were performed exactly as described previously [53; 76]. Except for the time course experiments, **5bk** was incubated overnight onto DRGs. In all cases, **5bk** was *also* added to the Tyrode solution during the loading with Fura-2AM. Fluorescence imaging was performed under the same conditions noted above for calcium imaging. A cell was defined as a “responder” if its fluorescence ratio of 340 nm/380 nm was greater than 10% of the baseline value calculated using the average fluorescence in the 30 seconds preceding application of the trigger.

2.7. Whole-cell patch recordings of Ca^{2+} and Na^{+} currents in acutely dissociated DRG neurons.

Recordings were obtained from acutely dissociated DRG neurons as described previously [34; 54]. The protocol for isolating T-type calcium currents was previously described by Choe et al.[14]

To isolate the contributions of the HVA calcium channel subtypes, we applied all but one of the following subunit-selective blockers (all purchased from Alomone Labs, Jerusalem): Nifedipine (10 μM, L-type); ω-agatoxin GIVA (200 nM, P/Q-type) [52]; SNX-482 (200 nM, R-type) [56]; ω-conotoxin GVIA (500 nM, N-type) [30] or TTA-P2 (1 μM, T-type)[14] to individually isolate the subtypes.

DRG neurons were interrogated with current-voltage (I-V) and activation/inactivation voltage protocols as previously described [17; 23].

2.8. Calcitonin gene–related peptide release from lumbar slices.

CGRP release was quantified as before [55].

2.9. Preparation of spinal cord slices.

As described previously [90], transverse 350-μm thick slices were prepared from young rats (postnatal 10–14 days) for electrophysiological recordings at RT. Slices were bathed in **5bk** for 2–3 hours prior to the recordings.

2.10. Electrophysiological recording in spinal cord slices by whole-cell patch clamp.

Substantia gelatinosa neurons were recorded from using methods exactly as described previously [91].

2.11. Implantation of intrathecal catheter.

For intrathecal (i.t.) drug administration, rats were chronically implanted with catheters as described by Yaksh and Rudy [89].

2.12. Testing of allodynia.

The assessment of tactile allodynia (i.e., a decreased threshold to paw withdrawal after probing with normally innocuous mechanical stimuli) using a series of calibrated fine (von Frey) filaments was done as described in Chaplan et al [11].

2.13. HIV sensory neuropathy (HIV SN).

Mechanical allodynia was produced by intrathecal administration of the human immunodeficiency virus-1 (HIV-1) envelope glycoprotein, GP120, as described [51]. Rats were tested on day 35 (i.e., 21 days after the last i.t. injection of GP120).

2.14. Paclitaxel-induced neuropathy model.

Neuropathy with paclitaxel (Cat# P-925–1, Goldbio, Olivette, MO) was induced with a final cumulative dose of 8 mg/kg using methods described earlier [60].

2.15. Elevated Plus Maze (EPM).

The EPM was used to calculate an anxiety index that combines notable parameters into one unified ratio with values ranging from 0 to 1, with a higher value indicating increased anxiety [33]. The following equation was used for calculation of the anxiety index:

Anxiety Index = 1 – (open arm time/5 min) + (open arm entry/total entry)

2.16. Spinal nerve ligation (SNL).

Nerve ligation, was performed as described earlier [40; 53].

2.17. Rotarod.

Rats were trained to walk on a rotating rod (10 rev/min; Rotamex 4/8 device) with a maximal cutoff time of 180 seconds as described before {Francois-Moutal, 2018 #14397}.

2.18. Competition Radioligand Binding

Details on our cell lines, culture methods, and binding methods have been reported previously [59]. The data was normalized to binding in the presence of Vehicle (100%; 0.1% DMSO and 0.1% BSA) and non-specific binding (0%; 10 μM naloxone) and reported as the mean ± SEM. Curves were fit using a 1-site binding 3-variable nonlinear regression model with GraphPad Prism 8.3, using the previously-measured K_D values of ^{3}H-diprenorphine in these cells [59].

2.19. Statistical Analysis.

All data was first tested for a Gaussian distribution using a D'Agostino-Pearson test (Prism 8 Software, Graphpad, San Diego, CA). SNI- (day 15 post-surgery), GP120- (day 15 post last injection) and paclitaxel- (day 15 post-injection) induced allodynia was quantified as percentage of maximum possible allodynia using the formula: percentage allodynia = [(baseline threshold − post-injury threshold)/baseline threshold] × 100. Reversal of allodynia by drugs (that is, anti-allodynia) was quantified with respect to the area under the threshold-time curve (using the trapezoidal method) over the post-injection testing period. Data are reported as percentage of the maximum possible anti-allodynia, calculated for each rat as a ratio of its actual anti-allodynia compared to a hypothetical situation in which the drug brought withdrawal thresholds to their original baseline at all post-injection time points. The statistical significance of differences between means was determined by a parametric ANOVA followed by Tukey's post hoc or a non-parametric Kruskal Wallis test followed by Dunn's post-hoc test depending on if datasets achieved normality. Behavioral data with a time course were analyzed by Two-way ANOVA with Sidak's post hoc test. Differences were considered significant if $p \leq 0.05$. Error bars in the graphs represent mean ± SEM. See statistical analysis described in Table 1. All data were plotted in Prism 8. No outlier data were removed.

3. Results

3.1. Chemical synthesis

All compounds were synthesized using the Ugi-azide four-component reaction methodology as shown in Supplementary Figure 1A. Chemical structures for the compounds tested in the Ca^{2+} flux assay are shown in Supplementary Figure 1B. Inspection of the chemical structure of **5bk** (Figure 1) did not reveal any significant metabolic and toxic liabilities, [72] as similar

structural components from **5bk** are also found in a number of FDA-approved oral drugs (Supplementary Figure 2).

5bk was not cytotoxic to either Madin-Darby Canine Kidney (MDCK) cells or adenocarcinomic human alveolar basal epithelial (A549) cells (cytotoxic concentration, CC_{50} > 100 μM) (data not shown).

3.2. Identification of compounds targeting low voltage-activated (LVA) calcium channels.

Using Fura 2-AM based ratiometric calcium-imaging assay as we have established before [23; 53; 54; 88], we screened an in-house diversity library of compounds (at 20 μM) for their ability to block Ca^{2+} influx via low (triggered with 40 mM KCl) and high (triggered with 90 mM KCl) voltage-activated calcium channels in primary rat dorsal root ganglion (DRG) neurons. The goal was to identify hits that inhibit LVA calcium channels but not high-voltage activated (HVA) calcium channels. In the first set, one compound, **5aa**, inhibited ~45% of the Ca^{2+} influx when DRGs were depolarized with 40 mM KCl and ~60% when depolarized with 90 mM KCl (Fig. 1A, B). As no compound in the initial round was selective for low voltage-activated calcium channels, we selected **5aa** for further optimization with the primary goal of achieving preferential activity towards LVA channels.

Encouraged by discovery of this initial hit, we subsequently synthesized a focused library of 45 analogs of **5aa** by varying the amine, aldehyde, and isocyanide components using the established Ugi-azide four-component reaction condition. The structures of the compounds are shown in Supplementary Figure 1B. Compounds **5ab**, **5ak**, **5al**, **5ao**, **5aq**, **5at**, **5aw**, **5ax**, **5ay**, **5ba**, **5be**, **5bh**, **5bi**, **5bp**, **5bq**, **5br**, **5bs**, and **5bt** were synthesized and tested as a diastereomer mixtures. Compounds **5bk** and **5bl** were tested as pure diastereomers and their absolute stereochemistry were confirmed by X-ray crystallography [94]. Three of the 46 compounds, **5ay**, **5bk**, and **5bt** inhibited >75% of Ca^{2+} influx when DRGs were depolarized with 40 mM KCl, of which 2 of these compounds **5ay** and **5bt** showed >50% inhibition when also triggered with 90 mM KCl (Fig. 1A, B). One compound, **5bk** (Fig. 1C) appeared selective in inhibiting KCl-evoked Ca^{2+} influx with 88.5 ± 2.6% inhibition (n=78) relative to the negative control (0.01% DMSO) when stimulated with 40 mM KCl and an ~33.9 ± 4.0 % inhibition (n=78) of evoked Ca^{2+} influx when stimulated with 90 mM KCl. The inhibition was observed only after at least 30 minutes of application of **5bk** and achieved a maximum with overnight treatment (Fig. 1D). The corresponding diastereomer, **5bl**, did not show significant inhibition of Ca^{2+} flux with < 25% signal reduction when DRGs were depolarized with either 40 mM or 90 mM KCl. Notably, compounds **5bk** and **5bl** were previously tested for their inhibition of the influenza virus polymerase PA-PB1 protein-protein interactions, and only compound **5bl** was found to be active [94]. These results suggest compound **5bk** targets LVA Ca^{2+} channels. Overall, compound **5bk** is the most potent and selective modulator against LVA Ca^{2+} channel among all the compounds tested.

We further analyzed the features of **5bk** antagonism, finding a concentration-dependent inhibition of LVA currents with an IC_{50} of 4.2 ± 0.6 μM (Fig. 1E). The inhibition was time-dependent with increasing block observed with longer incubation periods (Fig. 1D). **5bk**

also did not inhibit hERG channel at 100 μM in two-electrode voltage clamp assay, which has important implications for therapeutic safety (Supplementary Figure 3).

3.3. 5bk decreases T-type Ca^{2+} channels in sensory neurons.

One of the most potent hit compounds from the primary calcium imaging screening was **5bk** (Fig. 1), which showed nearly ~90% inhibition of Ca^{2+} channel influx at 20 μM when DRGs were depolarized with 40 mM KCl. As the inhibition of calcium influx elicited by **5bk** appeared to be more pronounced with 40 mM KCl versus 90 mM KCl (Fig. 1), we chose to test if T-type calcium channels were being preferentially targeted by this compound. In DRG sensory neurons, the α subunits of Cav3.2 and Cav3.3 represent the majority of T-type Ca^{2+} channels [93]. Therefore, we used electrophysiology protocols described before [14] to record T-type currents. From a holding potential of −90mV, we used 200-ms depolarization steps to change the membrane potential from −70 to +60 mV (10 mV increments) to evoke prototypical T-type calcium currents (Fig. 2A). After treatment with 0.01% DMSO (vehicle, n=16) or **5bk** (20 μM, n=16), we recorded low voltage-activated calcium currents (Fig. 2A) from DRG neurons with an average diameter between 20–30 μm. We measured current-voltage (I-V) relationships (Fig. 2B) and observed that treatment with **5bk** reduced T-type calcium current amplitudes between −20 mV and +10 mV test potentials (Fig. 2B). At peak current density (−10 mV), there was ~42.2% reduction in current in **5bk**-treated cells compared with vehicle-treated controls (Fig. 2C). Treatment with **5bk** did not alter the channel gating properties as we measured a similar half-maximal activation ($V_{0.5}$) of T-type calcium channels in both conditions (Fig. 2D). The kinetics of macroscopic current inactivation (Fig. 2E) were unchanged at all membrane potentials tested (−40 mV, Fig. 2F). The time-dependent activation (10 to 90% rise time) of T-type currents was not affected by treatment with **5bk** (Fig. 2G–H). We next tested whether **5bk** could control the voltage-dependent kinetics of channel inactivation (Fig. 2I) and found this property to also not be affected by treatment with **5bk**. Deactivating tail currents calculated using the single exponential function: $y = A1 \times e(-x/\tau 1) + y0$, where A1 is the amplitude, τ1 is the decay constant, and y0 is the offset. The resulting τ values (Fig. 2J), showed no differences irrespective of the treatment condition. Finally, because upon long membrane hyperpolarizations in DRG neurons T-type calcium channels can recover from inactivation, we tested if this biophysical parameter could be affected by treatment with **5bk**. This property has important consequences on the firing properties of sensory neurons expressing T-type calcium channels. Thus, we tested the recovery from inactivation using a double-pulse protocol with a variable interpulse duration at −90 mV (Fig. 2K) after a 500-ms-long inactivating pulse (Vh = −90 mV; Vt = −30 mV). T-type currents recovered fully, independently of the treatment condition (Fig. 2K). Taken together, our results show that **5bk** blocks T-type calcium channels in DRG neurons.

Given the lack of effect of **5bk** on the kinetic and voltage-dependent properties of T-type calcium currents, it is possible that **5bk** downregulates functional T-type channels by acting on second messenger pathways. To test this possibility, we applied **5bk** *acutely* during recordings. The results (Supplementary Figure 4), showed no inhibition of T-type currents, consistent with our data obtained from calcium imaging (Fig. 1D). Consequently, biophysical properties (i.e. voltage-activation, inactivation, recovery from inactivation) of

these LVA channels were also unaffected by **5bk** (Supplementary Figure 4). The complete lack of effect of acute perfusion of **5bk** on the amplitude and biophysical properties of T-type currents in DRG neurons (Supplementary Figure 4) suggests that **5bk** is not a blocker of T-type calcium channels but rather a regulator or modulator of T-type channel activity; **5bk** will be referred to interchangeably as regulator or modulator from here on.

To further explore selectivity of **5bk** for Cav3 over other HVA channel types, we examined how other channels were affected by **5bk** (Fig. 3). **5bk**, applied overnight, had no effect on pharmacologically isolated L-type (CaV1.x) (Fig. 3C, D), P/Q-type (CaV2.1) (Fig. 3H, I), N-type (CaV2.2) (Fig. 3M, N), or R-type (CaV2.3) (Fig. 3R, S) nor did it affect the $V_{1/2}$ of activation or inactivation (Fig. 3E, J, O, T and Supplementary Figure 5). Finally, we also observed no effects of **5bk** on tetrodotoxin-sensitive or -resistant voltage-gated sodium currents (Supplementary Figure 6).

3.4. 5bk modulates CaV3.2 T-type Ca^{2+}channels.

To test if **5bk** preferentially targets a specific T-type Ca^{2+} channel subunit we used a knockdown strategy (using short interfering RNA (siRNA)) to eliminate either CaV3.1, CaV3.2 or CaV3.3 in DRG sensory neurons (Fig. 4). DRG neurons were electroporated with the indicated siRNA (or a scrambled negative control) in combination with a GFP expressing plasmid (to identify transfected cells). The cells were cultured for 24 hours before adding 20μM of **5bk** overnight (or 0.1% DMSO as control) and then tested using 40 mM KCl as a trigger (Fig. 4). In scramble siRNA-transfected cells, **5bk** decreased 40 mM KCl evoked Ca^{2+} influx by ~53% (Fig. 4). In neurons with a knock down of CaV3.2, **5bk** failed to affect the 40 mM KCl evoked Ca^{2+} influx. In contrast, after the knockdown of either CaV3.1 or CaV3.3, significant decrement of calcium influx was still noted upon depolarization with 40 mM KCl (Fig. 4). Thus, we conclude that **5bk** preferentially regulates CaV3.2 Ca^{2+} channel subunits. A limitation of this approach is that the low expression of CaV3.1 or CaV3.3 in native DRG neurons may mask a potential broader regulatory action of **5bk**.

3.5. 5bk's effects on subpopulations of DRG neurons.

The data presented thus far demonstrates the potential for **5bk** to regulate Ca^{2+} influx via T-type Ca^{2+} channel. However, which cell-specific neuronal classes are implicated in **5bk**'s mechanism of action has not yet been addressed. In order to investigate this, we used the previously described constellation pharmacology protocol [75; 76] to explore cell-specific functionality as a result of key signaling proteins that define precise cell types. The constellation pharmacology assay poses 6 consecutive challenges, each 6 minutes apart, to compare Ca^{2+} influx due to activity of Ca^{2+}-associated membrane proteins: Ca^{2+} permeable ligand-gated ion channels, metabotropic receptors and voltage-gated Ca^{2+} channels. Following these 6 stimulations, KCl-evoked response due to membrane depolarization is used to assess viability of neurons; neurons not responsive to KCl are excluded from analysis.

The versatility in neuronal responsivity is demonstrated by exemplary traces of rat DRG sensory neurons treated with control (0.1% DMSO) or a 20 μM concentration of **5bk** as specified (Figs. 5A, B). Representative images of DMSO and **5bk**-treated neurons

(Supplementary Figs. 7, 8), show examples of calcium responses before and after challenge with each of the constellation triggers: menthol (400 nM), histamine (50 μM), ATP (10 μM), AITC (200 μM), acetylcholine (1 mM), capsaicin (100 nM) and KCl (90 mM)) during the constellation pharmacology protocol. Inhibition of Ca^{2+} influx due to KCl stimulus was again inhibited as a result of treatment with **5bk**; this is consistent with our previous data (Fig. 1). Sensory neurons were incubated overnight with the specified treatment, 0.01% DMSO (n=2002) or **5bk** (n=2902) and imaged the following day with the constellation pharmacology protocol. Data was collected from 5 independent experiments, and individual neuronal responses to each constellation trigger were analyzed. Neurons with responses under 10% of baseline fluorescence were excluded from the analyses.

We began with exploring the effect of **5bk** on the overall functionality of sensory neurons. This was analyzed in terms of functional cell subclasses present in the population of neurons treated with **5bk** in comparison to the control population. Notably, more functional subclasses were present in the population of neurons treated with **5bk** in comparison to those treated with vehicle control (Fig. 5C). However, response of neurons to the number of stimulatory challenges, independent of which specific agonists triggered response, was not altered by **5bk** treatment (Fig. 5D). Furthermore, we inquired whether **5bk** affected the sensitivity of DRGs to the different constellation triggers, by analyzing the percent of cells responding to a specific constellation trigger, independent of any other constellation triggers these neurons may have responded to. We noted an increased sensitivity to ATP stimulation and decreased sensitivity to capsaicin following treatment with **5bk** (Fig. 5E). Following treatment with **5bk**, there were no differences in functional cell subclasses including ATP or capsaicin as agonists (Fig. 5F).

In a more targeted inquiry, we also investigated the effect of **5bk** on the extent of Ca^{2+} influx following specific stimulation by each constellation trigger. Thus, we analyzed peak Ca^{2+} responses (Fig. 5G) and area under the curve (AUC) of these responses (Fig. 5H) in sensory neurons as a result of the specified treatment. We then asked if KCl-evoked Ca^{2+} response as a result of **5bk** would be altered in a functional-class specific manner (Fig. 5I). To test this, we assessed average peak Ca^{2+} response due to KCl challenge in sensory neurons that specifically responded to a particular constellation trigger, independent of any other constellation triggers that they might have responded to. Treatment with **5bk** significantly decreased KCl-evoked Ca^{2+} response in sensory neurons that responded to all but AITC and histamine responders (Fig. 5I). These results reveal the full mechanisms of Ca^{2+} inhibition by **5bk** and suggest its potential efficacy as an anti-nociceptive agent.

3.6. 5bk does not bind to the orthosteric site of the opioid receptors

To assess if **5bk** could work by off-target binding to the opioid receptors, we performed competition radioligand binding at all 3 opioid receptors in vitro. We competed **5bk** and a positive control compound (naloxone for MOR and DOR, U50,488 for KOR) vs. a fixed concentration of ^{3}H-diprenorphine in Chinese Hamster Ovary (CHO) cells expressing the human μ (MOR), δ (DOR), or κ (KOR) opioid receptor. We found that **5bk** did not bind to any opioid receptor up to a 10 μM concentration (Fig. 6A–C). In contrast, the positive control compounds bound to all 3 targets with expected affinity (Fig. 6A–C). These results

strongly suggest that **5bk** is not engaging the opioid receptors, and that potential anti-nociception would thus not be as a result of opioid receptor association.

3.7. 5bk inhibits spontaneous excitatory post-synaptic currents via presynaptic action.

Since T-type calcium channels contribute to action potential firing and neurotransmitter release [10], we performed electrophysiological recordings in substantia gelatinosa neurons in the superficial layers (within laminae I-II) of the spinal dorsal horn to measure whether **5bk** could inhibit spontaneous excitatory post-synaptic currents (sEPSCs). There was no significant decrease in spontaneous EPSC amplitude (post-synaptic effect) (Fig. 7A, B) of neurons treated with 0.1% DMSO or **5bk** (20 μM). However, **5bk** treatment (2–3 hours) decreased sEPSC frequency (DMSO, 1.96 ± 0.21 Hz; **5bk**, 1.26 ± 0.17 Hz, $P<0.05$) (Fig. 7C), suggesting a presynaptic suppression of neurotransmitter release by **5bk**.

3.8. 5bk inhibits calcitonin gene related peptide (CGRP) release in spinal cord slices.

Calcium entry via T-type Ca^{2+} channels contributes to the release of neurotransmitters, including CGRP, in the spinal dorsal horn.[63; 71; 79] Emergent evidence overall suggests that CGRP facilitates nociceptive transmission and contributes to development and maintenance of a sensitized, hyper-responsive state not only of the primary afferent sensory neurons but also of second-order pain transmission neurons within the CNS. This CGRP activity is thus thought to contribute to central sensitization as well. CGRP concentrations in spinal cords were measured directly via ELISA kits as described by us previously [7]. We observed that **5bk** inhibits KCl-evoked CGRP release from spinal cords, suggesting that **5bk** could be anti-nociceptive *in vivo* (Fig. 8).

3.9. Appraisal of 5bk in three models of neuropathy in rat

We used the spinal nerve ligation (SNL) model of neuropathic pain to evaluate the potential of **5bk** to reverse nociception. SNL injury efficiently reduced paw withdrawal thresholds (PWTs) (mechanical allodynia, Fig. 9A) 7 days post injury. Spinal administration of **5bk** significantly increased PWTs (Fig. 9A) for 2 hours during the course of the experiment. Transformation of the behavior data into percent anti-allodynia (see Methods) demonstrated a significant reversal of allodynia in rats injected with **5bk** (Fig. 9B). AUC analysis confirmed the reversal of mechanical allodynia (Fig. 9C) compared to vehicle-treated injured animals.

Of the many complications associated with both HIV and chemotherapy, a common symptom is HIV-induced sensory neuropathy and chemotherapy-induced peripheral neuropathy (CIPN) respectively [48]. Since voltage-gated Ca^{2+} channels have previously been found to contribute to neuropathic pain [57], we explored the potential utility of **5bk** in reversing the nociceptive effects induced by injections of the HIV envelope glycoprotein (gp120) or the chemotherapeutic drug paclitaxel. To test this, we first induced mechanical allodynia via 3 intrathecal injections of gp120, which has been shown to induce mechanical allodynia in animals[51; 92]; a subsequent reversal of mechanical allodynia by intrathecal injection of **5bk** (2 μg/5 μL) was seen at approximately 60 minutes post-gp120 injection and lasted for 4 hours (Fig. 9D). The same was true for the transformed data plotted as %anti-allodynia which was significantly reversed in rats injected with **5bk** (Fig. 9E). This reversal

of mechanical allodynia was also substantiated with a corresponding increase in area under the curve (Fig. 9F) associated with intrathecal administration of **5bk**.

Next, we assessed the effectiveness of intrathecally injected **5bk** (2 μg/5 μL) in ameliorating mechanical allodynia induced by a total of 4 paclitaxel injections (2mg/kg, intraperitoneal). Again, **5bk** resulted in a reversal of mechanical allodynia at two hours post-injection and lasting for at least two hours with a commensurate increase in area under the curve in comparison to saline-injected animals (Fig. 9G–I). Together, these results demonstrate that **5bk** is anti-nociceptive in rodent models of neuropathic pain.

3.10. 5bk does not alter motor function or anxiety levels in treated animals

Since **5bk** appears to be a promising anti-nociceptive agent in terms of neuropathic pain models, we next asked if the compound had any effects on motor function or anxiety in naïve animals. To test for motor deficits, we subjected rats to a rotarod performance test. Compared to vehicle-treated rats, there was no significant change in motor function in animals treated with intrathecal **5bk**. Vehicle-treated animals remained on the rotarod for an average of 172 ± 7.3 seconds (cutoff time 180 seconds per test) over a time-course of 300 minutes; **5bk**-treated animals remained on the rotarod for an average of 170 ± 9.6 seconds over a time-course of 300 minutes (Fig. 10A). From these results, we conclude that **5bk** does not induce motor deficits.

To test if anxiety levels are affected by **5bk**, we subjected naïve rats to the elevated plus maze (EPM) test. The measured anxiety index integrates both measurement of times and entries of the animals into the open and closed arms of the EPM. Index values closer to 1 indicate higher anxiety levels. Results indicate that there was no significant change in anxiety index between animals treated with **5bk** (2 μg/5 μL, i.t.) and those treated with vehicle (Fig. 10B), and thus we conclude that **5bk** is an anti-nociceptive agent that does not cause dysfunction in motor or anxiety-related measures.

4. Discussion

The present work used Ugi-azide MCR products to identify a modulator of the T-type Ca^{2+}channel. Of the 46 compounds tested, **5bk** - a benzimidazolonepiperidine analog, interacted with the T-type Ca^{2+} channels, specifically blocked T-type calcium channels in a concentration and time-dependent manner and preferentially inhibited the CaV3.2 isoform. **5bk** inhibited spinal neurotransmission which resulted in a decrease in CGRP release from the spinal cord. Finally, **5bk** had an anti-nociceptive effect in rodent models of neuropathic pain (Fig. 9) without inducing adverse side effects (Fig. 10). Taken together our findings indicate that the preferential modulation of T-type channels results in a selective and safe antinociceptive effect.

T-type Ca^{2+} channels were generally considered to regulate neuronal excitability at peripheral terminals of nociceptors, while high-voltage-activated (HVA) N- and P/Q- type Ca^{2+} channels regulate neurotransmitter release such as glutamate and substance P in the spinal cord [61]. The majority of studies examining T-type Ca^{2+} channels in the spinal cord have used less specific blockers such as ethosuximide [49], mibefradil [47] TTA-A2 and

TTA-P2 [35] to determine the function of the channels. However, there is evidence indicating that CaV3.2 channels regulate low-threshold exocytosis in cell cultures [85] and spontaneous release of glutamate in the spinal cord dorsal horn [35]. Unlike HVA Ca^{2+} channels, where several members of the vesicle release machinery interact with a synprint (synaptic protein interaction site) [62; 66], T-type Ca^{2+} channels lack the consensus synprint site. Therefore, the neurotransmitter release machine interacts with the C-terminal domain of the CaV3.2 channels for neurotransmitter release [84]. In the present study we show that selective blockade of the CaV3.2 channels plays an important role in excitatory synaptic transmission since **5bk** inhibited the frequency but not the amplitude of sEPSCs (Fig. 7). A decrease in frequency suggests that **5bk** inhibits glutamatergic excitatory inputs by a presynaptic mechanism. It is well accepted that alterations in the frequency of EPSCs with any agent targeting an ion channel indicates that this particular channel plays a presynaptic role, while changes in amplitude suggest a postsynaptic role of the channel. This is consistent with a previous report in which Jacus and colleagues demonstrated that CaV3.2 channels are the subtype of T-type Ca^{2+} channels responsible for presynaptic modulation of spontaneous synaptic transmission in lamina I and II [35]. Moreover, CaV3.2 channels appear not to participate in inhibitory synaptic transmission [35].

DRG neurons have been shown to differentially express T-type Ca^{2+} channels [64] with medium size neurons expressing the highest levels of CaV3.2 followed by small size neurons [67]. T-type Ca^{2+} currents are present in ~66 and ~42% of medium and small neurons, belonging to lightly myelinated Aδ and unmyelinated C fibers, respectively [4]. Small C-type fiber nociceptors can be subdivided according to the expression of histological markers [68; 73]. One group are the peptidergic fibers that express proinflammatory peptides such as CGRP and substance P and project to the most superficial layers of the spinal cord dorsal horn, lamina I and the outer lamina II. A second group, the nonpeptidergic fibers, can be identified by the presence of binding sites for the isolectin B4 (IB4) and do not express substance P nor CGRP. These C fibers project to inner lamina II of the spinal cord dorsal horn [68]. Among these fibers, CaV3.2 expresses preferentially in the CGRP neurons and to a lesser extent in IB4 positive fibers [35]. Importantly, our findings show that that **5bk** inhibited depolarization evoked CGRP release in spinal cord (Fig. 8), a known excitatory neurotransmitter that facilitates nociceptive transmission and contributes to central sensitization [68]. These results suggest a mechanism for the anti-nociceptive effect of **5bk** (Fig. 9).

CaV3.2 channel expression and activity is increased in DRG neurons and in the spinal cord dorsal horn in neuropathic pain, such as in the L5 spinal nerve cut [74], L5/L6 SNL [29], chronic constriction injury (CCI)[36], diabetic neuropathy [37; 50], paclitaxel-induced peripheral neuropathy [44], spared nerve injury (SNI)[38], chronic compression of DRGs [86], and partial sciatic nerve ligation (PSNL)[20] rodent models. Although changes in the open probability of CaV3.2 cannot be ruled out, the most straightforward explanation for a change in current density, as we showed in our results (Fig. 2), is that **5bk** decreases the cell surface or the protein expression of CaV3.2 channels. It is known that phosphorylation [5], glycosylation [83] and ubiquitylation [26] are two important post-translational regulation mechanisms that positively regulate surface expression of these channels.

It is also noteworthy that in neuropathic pain, there is a redistribution of the α2δ−1 HVA Ca^{2+} channels auxiliary subunit [2] and CaV3.2 channels [29] to the DRG of injured nerves. DRGs have been shown to be an ectopic activity generation sites that play an important role in the development and maintenance of neuropathic pain [45]. Similar to TRPV1 [25] and NaV1.8 channels [28], CaV3.2 channels are redistributed to uninjured nerves in neuropathic pain models. This contributes to spontaneous activity and suggests an important role in pain hypersensitivity [12; 46]. In our present study, we have demonstrated that preferential modulation of T-type channels with **5bk** reversed neuropathic pain (Fig. 9), which is consistent with previous reports of CaV3.2 silencing in DRGs of rats with CCI [4] and paclitaxel-induced peripheral neuropathy [38]. Interestingly, similar to mice lacking CaV3.2 [15], intrathecal administration of **5bk** had no alterations in motor function or anxiety (Fig. 10). However, a limitation here is that since **5bk** was administered intrathecally, it is possible that not enough of the compound may have reached the brain to engage CaV3.2 channels therein.

Finally, recent evidence from experiments involving recombinant T-channels indicate that the βγ subunit of G protein coupled receptors selectively inhibits the function of CaV3.2 channels by interacting with the intracellular loop connecting domains II and III and by decreasing single channel open probability [16]. Our findings suggested that **5bk** did not target G protein–coupled opioid receptor signaling (Fig. 6). Thus, a decrease of Ca^{2+} influx by **5bk** likely does not involve opioid receptors. Moreover, contrary to our previously identified CaV3.2 inhibitor betulinic acid [3], **5bk** did not affect any of the high voltage-activated calcium channels including N-type (CaV2.2) (Fig. 3), hERG channel activity (Supplementary Figure 3), or sodium channel activity (Supplementary Figure 6), which helps to confirm drug selectivity. In conclusion, the present study reports the identification of a new class of modulators of T-type Ca^{2+} channels, which may be further developed as promising candidates for efficacious, non-opioid pain therapeutics.

Supplementary Material

Refer to Web version on PubMed Central for supplementary material.

ACKNOWLEDGEMENTS

Jun Wang and Rajesh Khanna are co-senior authors. This work was supported by National Institutes of Health awards (R01NS098772 from the National Institute of Neurological Disorders and Stroke and R01DA042852 from the National Institute on Drug Abuse to R.K., and the Arizona Biomedical Research Centre new investigator award grant ADHS18-198859 and grants AI119187 and AI144887 from the National Institute of Allergy and Infectious Diseases to J.W.) and a NIH HEAL award (1R41NS116784-01 from the National Institute of Neurological Disorders and Stroke to Regulonix LLC (R. Khanna).

ABBREVIATIONS USED

A549	adenocarcinomic human alveolar basal epithelial cells
AITC	Allyl isothiocyanate
CaV3	voltage-gated calcium channel subfamily 3

CC50	cytotoxic concentration
CGRP	calcitonin gene-related peptide
CHO	Chinese Hamster Ovary
CIPN	chemotherapy-induced peripheral neuropathy
DOR	delta opioid receptor
DRG	dorsal root ganglia
EPM	elevated plus maze
hERG	human Ether-a-go-go-Related gene, codes for Kv11.1 channel
HIV gp120	human immunodeficiency virus envelope glycoprotein
KOR	kappa opioid receptor
KCl	potassium chloride
LVA	low voltage-activated
MOR	mu opioid receptor
MCR	multicomponent reactions
MDCK	Madin-Darby Canine Kidney cells
sEPSCs	spontaneous excitatory post-synaptic currents
HVA	high-voltage-activated
IB4	isolectin B4
CCI	chronic constriction injury
SNI	spared nerve injury
PSNL	partial sciatic nerve ligation
5bk	1-{1-[(R)-{1-[(1S)-1-phenylethyl]-1,2,3,4-tetrazol-5-yl}(thiophen-3-yl)methyl]piperidin-4-yl}-3H-1,3-benzodiazol-2-one

REFERENCES

[1]. Aziz-Donnelly A, Harrison TB. Update of HIV-Associated Sensory Neuropathies. Curr Treat Options Neurol 2017;19(10):36. [PubMed: 28861848]

[2]. Bauer CS, Rahman W, Tran-van-Minh A, Lujan R, Dickenson AH, Dolphin AC. The anti-allodynic alpha(2)delta ligand pregabalin inhibits the trafficking of the calcium channel alpha(2)delta-1 subunit to presynaptic terminals in vivo. Biochemical Society transactions 2010;38(2):525–528. [PubMed: 20298215]

[3]. Bellampalli SS, Ji Y, Moutal A, Cai S, Wijeratne EMK, Gandini MA, Yu J, Chefdeville A, Dorame A, Chew LA, Madura CL, Luo S, Molnar G, Khanna M, Streicher JM, Zamponi GW, Gunatilaka AAL, Khanna R. Betulinic acid, derived from the desert lavender Hyptis emoryi, attenuates

paclitaxel-, HIV-, and nerve injury-associated peripheral sensory neuropathy via block of N- and T-type calcium channels. Pain 2019;160(1):117–135. [PubMed: 30169422]

[4]. Bernal Sierra YA, Haseleu J, Kozlenkov A, Begay V, Lewin GR. Genetic Tracing of Cav3.2 T-Type Calcium Channel Expression in the Peripheral Nervous System. Frontiers in molecular neuroscience 2017;10:70. [PubMed: 28360836]

[5]. Blesneac I, Chemin J, Bidaud I, Huc-Brandt S, Vandermoere F, Lory P. Phosphorylation of the Cav3.2 T-type calcium channel directly regulates its gating properties. Proceedings of the National Academy of Sciences of the United States of America 2015;112(44):13705–13710. [PubMed: 26483470]

[6]. Bourinet E, Alloui A, Monteil A, Barrere C, Couette B, Poirot O, Pages A, McRory J, Snutch TP, Eschalier A, Nargeot J. Silencing of the Cav3.2 T-type calcium channel gene in sensory neurons demonstrates its major role in nociception. EMBO J 2005;24(2):315–324. [PubMed: 15616581]

[7]. Brittain JM, Duarte DB, Wilson SM, Zhu W, Ballard C, Johnson PL, Liu N, Xiong W, Ripsch MS, Wang Y, Fehrenbacher JC, Fitz SD, Khanna M, Park CK, Schmutzler BS, Cheon BM, Due MR, Brustovetsky T, Ashpole NM, Hudmon A, Meroueh SO, Hingtgen CM, Brustovetsky N, Ji RR, Hurley JH, Jin X, Shekhar A, Xu XM, Oxford GS, Vasko MR, White FA, Khanna R. Suppression of inflammatory and neuropathic pain by uncoupling CRMP-2 from the presynaptic Ca(2)(+) channel complex. Nature medicine 2011;17(7):822–829.

[8]. Calvo M, Davies AJ, Hebert HL, Weir GA, Chesler EJ, Finnerup NB, Levitt RC, Smith BH, Neely GG, Costigan M, Bennett DL. The Genetics of Neuropathic Pain from Model Organisms to Clinical Application. Neuron 2019;104(4):637–653. [PubMed: 31751545]

[9]. Candelas M, Reynders A, Arango-Lievano M, Neumayer C, Fruquiere A, Demes E, Hamid J, Lemmers C, Bernat C, Monteil A, Compan V, Laffray S, Inquimbert P, Le Feuvre Y, Zamponi GW, Moqrich A, Bourinet E, Mery PF. Cav3.2 T-type calcium channels shape electrical firing in mouse Lamina II neurons. Sci Rep 2019;9(1):3112. [PubMed: 30816223]

[10]. Catterall WA. Structure and function of neuronal Ca2+ channels and their role in neurotransmitter release. Cell calcium 1998;24(5–6):307–323. [PubMed: 10091001]

[11]. Chaplan SR, Bach FW, Pogrel JW, Chung JM, Yaksh TL. Quantitative assessment of tactile allodynia in the rat paw. Journal of neuroscience methods 1994;53(1):55–63. [PubMed: 7990513]

[12]. Chen W, Chi YN, Kang XJ, Liu QY, Zhang HL, Li ZH, Zhao ZF, Yang Y, Su L, Cai J, Liao FF, Yi M, Wan Y, Liu FY. Accumulation of Cav3.2 T-type Calcium Channels in the Uninjured Sural Nerve Contributes to Neuropathic Pain in Rats with Spared Nerve Injury. Frontiers in molecular neuroscience 2018;11:24. [PubMed: 29472842]

[13]. Chen YL, Tsaur ML, Wang SW, Wang TY, Hung YC, Lin CS, Chang YF, Wang YC, Shiue SJ, Cheng JK. Chronic intrathecal infusion of mibefradil, ethosuximide and nickel attenuates nerve ligation-induced pain in rats. British journal of anaesthesia 2015;115(1):105–111. [PubMed: 26089446]

[14]. Choe W, Messinger RB, Leach E, Eckle VS, Obradovic A, Salajegheh R, Jevtovic-Todorovic V, Todorovic SM. TTA-P2 is a potent and selective blocker of T-type calcium channels in rat sensory neurons and a novel antinociceptive agent. MolPharmacol 2011;80(5):900–910.

[15]. Choi S, Na HS, Kim J, Lee J, Lee S, Kim D, Park J, Chen CC, Campbell KP, Shin HS. Attenuated pain responses in mice lacking Ca(V)3.2 T-type channels. Genes Brain Behav 2007;6(5):425–431. [PubMed: 16939637]

[16]. DePuy SD, Yao J, Hu C, McIntire W, Bidaud I, Lory P, Rastinejad F, Gonzalez C, Garrison JC, Barrett PQ. The molecular basis for T-type Ca2+ channel inhibition by G protein beta2gamma2 subunits. Proceedings of the National Academy of Sciences of the United States of America 2006;103(39):14590–14595. [PubMed: 16973746]

[17]. Dustrude ET, Moutal A, Yang X, Wang Y, Khanna M, Khanna R. Hierarchical CRMP2 posttranslational modifications control NaV1.7 function. Proceedings of the National Academy of Sciences of the United States of America 2016;113(52):E8443–E8452. [PubMed: 27940916]

[18]. Dustrude ET, Wilson SM, Ju W, Xiao Y, Khanna R. CRMP2 protein SUMOylation modulates NaV1.7 channel trafficking. The Journal of biological chemistry 2013;288(34):24316–24331. [PubMed: 23836888]

[19]. Egan MF, Zhao X, Smith A, Troyer MD, Uebele VN, Pidkorytov V, Cox K, Murphy M, Snavely D, Lines C, Michelson D. Randomized controlled study of the T-type calcium channel antagonist MK-8998 for the treatment of acute psychosis in patients with schizophrenia. Hum Psychopharmacol 2013;28(2):124–133. [PubMed: 23532746]

[20]. Feng XJ, Ma LX, Jiao C, Kuang HX, Zeng F, Zhou XY, Cheng XE, Zhu MY, Zhang DY, Jiang CY, Liu T. Nerve injury elevates functional Cav3.2 channels in superficial spinal dorsal horn. Molecular pain 2019;15:1744806919836569. [PubMed: 30803310]

[21]. Flatters SJ, Bennett GJ. Ethosuximide reverses paclitaxel- and vincristine-induced painful peripheral neuropathy. Pain 2004;109(1–2):150–161. [PubMed: 15082137]

[22]. Francois A, Schuetter N, Laffray S, Sanguesa J, Pizzoccaro A, Dubel S, Mantilleri A, Nargeot J, Noel J, Wood JN, Moqrich A, Pongs O, Bourinet E. The Low-Threshold Calcium Channel Cav3.2 Determines Low-Threshold Mechanoreceptor Function. Cell Rep 2015.

[23]. Francois-Moutal L, Wang Y, Moutal A, Cottier KE, Melemedjian OK, Yang X, Wang Y, Ju W, Largent-Milnes TM, Khanna M, Vanderah TW, Khanna R. A membrane-delimited N-myristoylated CRMP2 peptide aptamer inhibits CaV2.2 trafficking and reverses inflammatory and postoperative pain behaviors. Pain 2015;156(7):1247–1264. [PubMed: 25782368]

[24]. Friesner RA, Banks JL, Murphy RB, Halgren TA, Klicic JJ, Mainz DT, Repasky MP, Knoll EH, Shelley M, Perry JK, Shaw DE, Francis P, Shenkin PS. Glide: a new approach for rapid, accurate docking and scoring. 1. Method and assessment of docking accuracy. Journal of medicinal chemistry 2004;47(7):1739–1749. [PubMed: 15027865]

[25]. Fukuoka T, Yamanaka H, Kobayashi K, Okubo M, Miyoshi K, Dai Y, Noguchi K. Re-evaluation of the phenotypic changes in L4 dorsal root ganglion neurons after L5 spinal nerve ligation. Pain 2012;153(1):68–79. [PubMed: 22054598]

[26]. Garcia-Caballero A, Gadotti VM, Stemkowski P, Weiss N, Souza IA, Hodgkinson V, Bladen C, Chen L, Hamid J, Pizzoccaro A, Deage M, Francois A, Bourinet E, Zamponi GW. The deubiquitinating enzyme USP5 modulates neuropathic and inflammatory pain by enhancing Cav3.2 channel activity. Neuron 2014;83(5):1144–1158. [PubMed: 25189210]

[27]. Girach A, Julian TH, Varrassi G, Paladini A, Vadalouka A, Zis P. Quality of Life in Painful Peripheral Neuropathies: A Systematic Review. Pain Res Manag 2019;2019:2091960. [PubMed: 31249636]

[28]. Gold MS, Weinreich D, Kim CS, Wang R, Treanor J, Porreca F, Lai J. Redistribution of Na(V)1.8 in uninjured axons enables neuropathic pain. The Journal of neuroscience : the official journal of the Society for Neuroscience 2003;23(1):158–166. [PubMed: 12514212]

[29]. Gomez K, Calderon-Rivera A, Sandoval A, Gonzalez-Ramirez R, Vargas-Parada A, Ojeda-Alonso J, Granados-Soto V, Delgado-Lezama R, Felix R. Cdk5-Dependent Phosphorylation of CaV3.2 T-Type Channels: Possible Role in Nerve Ligation-Induced Neuropathic Allodynia and the Compound Action Potential in Primary Afferent C Fibers. The Journal of neuroscience : the official journal of the Society for Neuroscience 2020;40(2):283–296. [PubMed: 31744861]

[30]. Gray WR, Olivera BM, Cruz LJ. Peptide toxins from venomous Conus snails. Annual review of biochemistry 1988;57:665–700.

[31]. Hamidi GA, Ramezani MH, Arani MN, Talaei SA, Mesdaghinia A, Banafshe HR. Ethosuximide reduces allodynia and hyperalgesia and potentiates morphine effects in the chronic constriction injury model of neuropathic pain. European journal of pharmacology 2012;674(2–3):260–264. [PubMed: 22134003]

[32]. Head J, Mazza J, Sabourin V, Turpin J, Hoelscher C, Wu C, Sharan A. Waves of Pain Relief: A Systematic Review of Clinical Trials in Spinal Cord Stimulation Waveforms for the Treatment of Chronic Neuropathic Low Back and Leg Pain. World Neurosurg 2019;131:264–274 e263. [PubMed: 31369885]

[33]. Huynh TN, Krigbaum AM, Hanna JJ, Conrad CD. Sex differences and phase of light cycle modify chronic stress effects on anxiety and depressive-like behavior. Behavioural brain research 2011;222(1):212–222. [PubMed: 21440009]

[34]. Ibrahim MM, Patwardhan A, Gilbraith KB, Moutal A, Yang X, Chew LA, Largent-Milnes T, Malan TP, Vanderah TW, Porreca F, Khanna R. Long-lasting antinociceptive effects of green light in acute and chronic pain in rats. Pain 2017;158(2):347–360. [PubMed: 28092651]

[35]. Jacus MO, Uebele VN, Renger JJ, Todorovic SM. Presynaptic Cav3.2 channels regulate excitatory neurotransmission in nociceptive dorsal horn neurons. The Journal of neuroscience : the official journal of the Society for Neuroscience 2012;32(27):9374–9382. [PubMed: 22764245]

[36]. Jagodic MM, Pathirathna S, Joksovic PM, Lee W, Nelson MT, Naik AK, Su P, Jevtovic-Todorovic V, Todorovic SM. Upregulation of the T-type calcium current in small rat sensory neurons after chronic constrictive injury of the sciatic nerve. JNeurophysiol 2008;99(6):3151–3156. [PubMed: 18417624]

[37]. Jagodic MM, Pathirathna S, Nelson MT, Mancuso S, Joksovic PM, Rosenberg ER, Bayliss DA, Jevtovic-Todorovic V, Todorovic SM. Cell-specific alterations of T-type calcium current in painful diabetic neuropathy enhance excitability of sensory neurons. JNeurosci 2007;27(12):3305–3316. [PubMed: 17376991]

[38]. Kang XJ, Chi YN, Chen W, Liu FY, Cui S, Liao FF, Cai J, Wan Y. Increased expression of CaV3.2 T-type calcium channels in damaged DRG neurons contributes to neuropathic pain in rats with spared nerve injury. Molecular pain 2018;14:1744806918765808. [PubMed: 29592785]

[39]. Kelley LA, Mezulis S, Yates CM, Wass MN, Sternberg MJ. The Phyre2 web portal for protein modeling, prediction and analysis. Nature protocols 2015;10(6):845–858. [PubMed: 25950237]

[40]. Khanna R, Yu J, Yang X, Moutal A, Chefdeville A, Gokhale V, Shuja Z, Chew LA, Bellampalli SS, Luo S, Francois-Moutal L, Serafini MJ, Ha T, Perez-Miller S, Park KD, Patwardhan A, Streicher JM, Colecraft HM, Khanna M. Targeting the CaVα-β interaction yields an antagonist of the N-type CaV2.2 channel with broad antinociceptive efficacy. Pain 2019.

[41]. Lambert RC, Bessaih T, Leresche N. Modulation of neuronal T-type calcium channels. CNSNeurolDisordDrug Targets 2006;5(6):611–627.

[42]. Lee M Z944: a first in class T-type calcium channel modulator for the treatment of pain. Journal of the peripheral nervous system : JPNS 2014;19 Suppl 2:S11–12. [PubMed: 25269728]

[43]. Leresche N, Lambert RC. T-type calcium channels in synaptic plasticity. Channels (Austin) 2017;11(2):121–139. [PubMed: 27653665]

[44]. Li Y, Tatsui CE, Rhines LD, North RY, Harrison DS, Cassidy RM, Johansson CA, Kosturakis AK, Edwards DD, Zhang H, Dougherty PM. Dorsal root ganglion neurons become hyperexcitable and increase expression of voltage-gated T-type calcium channels (Cav3.2) in paclitaxel-induced peripheral neuropathy. Pain 2017;158(3):417–429. [PubMed: 27902567]

[45]. Liu CN, Wall PD, Ben-Dor E, Michaelis M, Amir R, Devor M. Tactile allodynia in the absence of C-fiber activation: altered firing properties of DRG neurons following spinal nerve injury. Pain 2000;85(3):503–521. [PubMed: 10781925]

[46]. Liu QY, Chen W, Cui S, Liao FF, Yi M, Liu FY, Wan Y. Upregulation of Cav3.2 T-type calcium channels in adjacent intact L4 dorsal root ganglion neurons in neuropathic pain rats with L5 spinal nerve ligation. Neurosci Res 2019;142:30–37. [PubMed: 29684385]

[47]. Maeda Y, Aoki Y, Sekiguchi F, Matsunami M, Takahashi T, Nishikawa H, Kawabata A. Hyperalgesia induced by spinal and peripheral hydrogen sulfide: evidence for involvement of Cav3.2 T-type calcium channels. Pain 2009;142(1–2):127–132. [PubMed: 19167819]

[48]. Manji H Neuropathy in HIV infection. Current opinion in neurology 2000;13(5):589–592. [PubMed: 11073368]

[49]. Matthews EA, Dickenson AH. Effects of spinally delivered N- and P-type voltage-dependent calcium channel antagonists on dorsal horn neuronal responses in a rat model of neuropathy. Pain 2001;92(1–2):235–246. [PubMed: 11323145]

[50]. Messinger RB, Naik AK, Jagodic MM, Nelson MT, Lee WY, Choe WJ, Orestes P, Latham JR, Todorovic SM, Jevtovic-Todorovic V. In vivo silencing of the Ca(V)3.2 T-type calcium channels in sensory neurons alleviates hyperalgesia in rats with streptozocin-induced diabetic neuropathy. Pain 2009;145(1–2):184–195. [PubMed: 19577366]

[51]. Milligan ED, O'Connor KA, Nguyen KT, Armstrong CB, Twining C, Gaykema RP, Holguin A, Martin D, Maier SF, Watkins LR. Intrathecal HIV-1 envelope glycoprotein gp120 induces enhanced pain states mediated by spinal cord proinflammatory cytokines. The Journal of neuroscience : the official journal of the Society for Neuroscience 2001;21(8):2808–2819. [PubMed: 11306633]

[52]. Mintz IM, Venema VJ, Swiderek KM, Lee TD, Bean BP, Adams ME. P-type calcium channels blocked by the spider toxin omega-Aga-IVA. Nature 1992;355(6363):827–829. [PubMed: 1311418]

[53]. Moutal A, Chew LA, Yang X, Wang Y, Yeon SK, Telemi E, Meroueh S, Park KD, Shrinivasan R, Gilbraith KB, Qu C, Xie JY, Patwardhan A, Vanderah TW, Khanna M, Porreca F, Khanna R. (S)-lacosamide inhibition of CRMP2 phosphorylation reduces postoperative and neuropathic pain behaviors through distinct classes of sensory neurons identified by constellation pharmacology. Pain 2016;157(7):1448–1463. [PubMed: 26967696]

[54]. Moutal A, Li W, Wang Y, Ju W, Luo S, Cai S, Francois-Moutal L, Perez-Miller S, Hu J, Dustrude ET, Vanderah TW, Gokhale V, Khanna M, Khanna R. Homology-guided mutational analysis reveals the functional requirements for antinociceptive specificity of collapsin response mediator protein 2-derived peptides. British journal of pharmacology 2017.

[55]. Moutal A, Wang Y, Yang X, Ji Y, Luo S, Dorame A, Bellampalli SS, Chew LA, Cai S, Dustrude ET, Keener JE, Marty MT, Vanderah TW, Khanna R. Dissecting the role of the CRMP2-neurofibromin complex on pain behaviors. Pain 2017;158(11):2203–2221. [PubMed: 28767512]

[56]. Newcomb R, Szoke B, Palma A, Wang G, Chen X, Hopkins W, Cong R, Miller J, Urge L, Tarczy-Hornoch K, Loo JA, Dooley DJ, Nadasdi L, Tsien RW, Lemos J, Miljanich G. Selective peptide antagonist of the class E calcium channel from the venom of the tarantula Hysterocrates gigas. Biochemistry 1998;37(44):15353–15362. [PubMed: 9799496]

[57]. Newshan G HIV neuropathy treated with gabapentin. AIDS 1998;12(2):219–221. [PubMed: 9468374]

[58]. Okubo K, Takahashi T, Sekiguchi F, Kanaoka D, Matsunami M, Ohkubo T, Yamazaki J, Fukushima N, Yoshida S, Kawabata A. Inhibition of T-type calcium channels and hydrogen sulfide-forming enzyme reverses paclitaxel-evoked neuropathic hyperalgesia in rats. Neuroscience 2011;188:148–56. Epub;%2011 May 11.:148–156. [PubMed: 21596106]

[59]. Olson KM, Duron DI, Womer D, Fell R, Streicher JM. Comprehensive molecular pharmacology screening reveals potential new receptor interactions for clinically relevant opioids. PloS one 2019;14(6):e0217371. [PubMed: 31170174]

[60]. Polomano RC, Mannes AJ, Clark US, Bennett GJ. A painful peripheral neuropathy in the rat produced by the chemotherapeutic drug, paclitaxel. Pain 2001;94(3):293–304. [PubMed: 11731066]

[61]. Reid CA, Clements JD, Bekkers JM. Nonuniform distribution of Ca2+ channel subtypes on presynaptic terminals of excitatory synapses in hippocampal cultures. JNeurosci 1997;17(8):2738–2745. [PubMed: 9092595]

[62]. Rettig J, Sheng ZH, Kim DK, Hodson CD, Snutch TP, Catterall WA. Isoform-specific interaction of the alpha1A subunits of brain Ca2+ channels with the presynaptic proteins syntaxin and SNAP-25. ProcNatlAcadSciUSA 1996;93(14):7363–7368.

[63]. Rose KE, Lunardi N, Boscolo A, Dong X, Erisir A, Jevtovic-Todorovic V, Todorovic SM. Immunohistological demonstration of CaV3.2 T-type voltage-gated calcium channel expression in soma of dorsal root ganglion neurons and peripheral axons of rat and mouse. Neuroscience 2013;250:263–274. [PubMed: 23867767]

[64]. Scroggs RS, Fox AP. Calcium current variation between acutely isolated adult rat dorsal root ganglion neurons of different size. JPhysiol 1992;445:639–58.:639–658. [PubMed: 1323671]

[65]. Sekiguchi F, Kawara Y, Tsubota M, Kawakami E, Ozaki T, Kawaishi Y, Tomita S, Kanaoka D, Yoshida S, Ohkubo T, Kawabata A. Therapeutic potential of RQ-00311651, a novel T-type Ca2+ channel blocker, in distinct rodent models for neuropathic and visceral pain. Pain 2016;157(8):1655–1665. [PubMed: 27023424]

[66]. Sheng ZH, Rettig J, Cook T, Catterall WA. Calcium-dependent interaction of N-type calcium channels with the synaptic core complex. Nature 1996;379(6564):451–454. [PubMed: 8559250]

[67]. Shin JB, Martinez-Salgado C, Heppenstall PA, Lewin GR. A T-type calcium channel required for normal function of a mammalian mechanoreceptor. NatNeurosci 2003;6(7):724–730.

[68]. Snider WD, McMahon SB. Tackling pain at the source: new ideas about nociceptors. Neuron 1998;20(4):629–632. [PubMed: 9581756]

[69]. Snutch TP, Zamponi GW. Recent advances in the development of T-type calcium channel blockers for pain intervention. British journal of pharmacology 2017.

[70]. Staff NP, Fehrenbacher JC, Caillaud M, Damaj MI, Segal RA, Rieger S. Pathogenesis of paclitaxel-induced peripheral neuropathy: A current review of in vitro and in vivo findings using rodent and human model systems. Exp Neurol 2019;324:113121. [PubMed: 31758983]

[71]. Stemkowski P, Garcia-Caballero A, Gadotti VM, M'Dahoma S, Huang S, Black SA, Chen L, Souza IA, Zhang Z, Zamponi GW. TRPV1 Nociceptor Activity Initiates USP5/T-type Channel-Mediated Plasticity. Cell Rep 2016;17(11):2901–2912. [PubMed: 27974205]

[72]. Stepan AF, Walker DP, Bauman J, Price DA, Baillie TA, Kalgutkar AS, Aleo MD. Structural Alert/Reactive Metabolite Concept as Applied in Medicinal Chemistry to Mitigate the Risk of Idiosyncratic Drug Toxicity: A Perspective Based on the Critical Examination of Trends in the Top 200 Drugs Marketed in the United States. Chem Res Toxicol 2011;24(9):1345–1410. [PubMed: 21702456]

[73]. Stucky CL, Lewin GR. Isolectin B(4)-positive and -negative nociceptors are functionally distinct. The Journal of neuroscience : the official journal of the Society for Neuroscience 1999;19(15):6497–6505. [PubMed: 10414978]

[74]. Takahashi T, Aoki Y, Okubo K, Maeda Y, Sekiguchi F, Mitani K, Nishikawa H, Kawabata A. Upregulation of Ca(v)3.2 T-type calcium channels targeted by endogenous hydrogen sulfide contributes to maintenance of neuropathic pain. Pain 2010;150(1):183–191. [PubMed: 20546998]

[75]. Teichert RW, Memon T, Aman JW, Olivera BM. Using constellation pharmacology to define comprehensively a somatosensory neuronal subclass. Proceedings of the National Academy of Sciences of the United States of America 2014;111(6):2319–2324. [PubMed: 24469798]

[76]. Teichert RW, Schmidt EW, Olivera BM. Constellation pharmacology: a new paradigm for drug discovery. Annual review of pharmacology and toxicology 2015;55:573–589.

[77]. Teleb M, Zhang FX, Huang J, Gadotti VM, Farghaly AM, AboulWafa OM, Zamponi GW, Fahmy H. Synthesis and biological evaluation of novel N3-substituted dihydropyrimidine derivatives as T-type calcium channel blockers and their efficacy as analgesics in mouse models of inflammatory pain. Bioorganic & medicinal chemistry 2017;25(6):1926–1938. [PubMed: 28233679]

[78]. Todorovic SM, Jevtovic-Todorovic V. T-type voltage-gated calcium channels as targets for the development of novel pain therapies. British journal of pharmacology 2011;163(3):484–495. [PubMed: 21306582]

[79]. Todorovic SM, Jevtovic-Todorovic V. Neuropathic pain: role for presynaptic T-type channels in nociceptive signaling. Pflugers Archiv : European journal of physiology 2013;465(7):921–927. [PubMed: 23322114]

[80]. Tringham E, Powell KL, Cain SM, Kuplast K, Mezeyova J, Weerapura M, Eduljee C, Jiang X, Smith P, Morrison JL, Jones NC, Braine E, Rind G, Fee-Maki M, Parker D, Pajouhesh H, Parmar M, O'Brien TJ, Snutch TP. T-type calcium channel blockers that attenuate thalamic burst firing and suppress absence seizures. Science translational medicine 2012;4(121):121ra119.

[81]. Waxman SG, Zamponi GW. Regulating excitability of peripheral afferents: emerging ion channel targets. Nature neuroscience 2014;17(2):153–163. [PubMed: 24473263]

[82]. Webster LR, Fakata KL, Charapata S, Fisher R, MineHart M. Open-label, multicenter study of combined intrathecal morphine and ziconotide: addition of morphine in patients receiving ziconotide for severe chronic pain. Pain Med 2008;9(3):282–290. [PubMed: 18366508]

[83]. Weiss N, Black SA, Bladen C, Chen L, Zamponi GW. Surface expression and function of Cav3.2 T-type calcium channels are controlled by asparagine-linked glycosylation. Pflugers Archiv : European journal of physiology 2013;465(8):1159–1170. [PubMed: 23503728]

[84]. Weiss N, Hameed S, Fernandez-Fernandez JM, Fablet K, Karmazinova M, Poillot C, Proft J, Chen L, Bidaud I, Monteil A, Huc-Brandt S, Lacinova L, Lory P, Zamponi GW, De Waard M. A Ca(v)3.2/syntaxin-1A signaling complex controls T-type channel activity and low-threshold exocytosis. The Journal of biological chemistry 2012;287(4):2810–2818. [PubMed: 22130660]

[85]. Weiss N, Zamponi GW. Control of low-threshold exocytosis by T-type calcium channels. Biochimica et biophysica acta 2012.

[86]. Wen XJ, Xu SY, Chen ZX, Yang CX, Liang H, Li H. The roles of T-type calcium channel in the development of neuropathic pain following chronic compression of rat dorsal root ganglia. Pharmacology 2010;85(5):295–300. [PubMed: 20453553]

[87]. Xiao W, Naso L, Bennett GJ. Experimental studies of potential analgesics for the treatment of chemotherapy-evoked painful peripheral neuropathies. Pain Med 2008;9(5):505–517. [PubMed: 18777607]

[88]. Xie JY, Chew LA, Yang X, Wang Y, Qu C, Wang Y, Federici LM, Fitz SD, Ripsch MS, Due MR, Moutal A, Khanna M, White FA, Vanderah TW, Johnson PL, Porreca F, Khanna R. Sustained relief of ongoing experimental neuropathic pain by a CRMP2 peptide aptamer with low abuse potential. Pain 2016;157(9):2124–2140. [PubMed: 27537210]

[89]. Yaksh TL, Rudy TA. Chronic catheterization of the spinal subarachnoid space. Physiology & behavior 1976;17(6):1031–1036. [PubMed: 14677603]

[90]. Yu J, Moutal A, Dorame A, Bellampalli SS, Chefdeville A, Kanazawa I, Pham NYN, Park KD, Weimer JM, Khanna R. Phosphorylated CRMP2 Regulates Spinal Nociceptive Neurotransmission. Molecular neurobiology 2018.

[91]. Yu J, Moutal A, Dorame A, Bellampalli SS, Chefdeville A, Kanazawa I, Pham NYN, Park KD, Weimer JM, Khanna R. Phosphorylated CRMP2 Regulates Spinal Nociceptive Neurotransmission. Molecular neurobiology 2019;56(7):5241–5255. [PubMed: 30565051]

[92]. Yuan SB, Shi Y, Chen J, Zhou X, Li G, Gelman BB, Lisinicchia JG, Carlton SM, Ferguson MR, Tan A, Sarna SK, Tang SJ. Gp120 in the pathogenesis of human immunodeficiency virus-associated pain. Annals of neurology 2014;75(6):837–850. [PubMed: 24633867]

[93]. Yue J, Liu L, Liu Z, Shu B, Zhang Y. Upregulation of T-type Ca2+ channels in primary sensory neurons in spinal nerve injury. Spine (Phila Pa 1976) 2013;38(6):463–470. [PubMed: 22972512]

[94]. Zhang J, Hu Y, Foley C, Wang Y, Musharrafieh R, Xu S, Zhang Y, Ma C, Hulme C, Wang J. Exploring Ugi-Azide Four-Component Reaction Products for Broad-Spectrum Influenza Antivirals with a High Genetic Barrier to Drug Resistance. Sci Rep 2018;8(1):4653. [PubMed: 29545578]

[95]. Zhao Y, Huang G, Wu Q, Wu K, Li R, Lei J, Pan X, Yan N. Cryo-EM structures of apo and antagonist-bound human Cav3.1. Nature 2019.

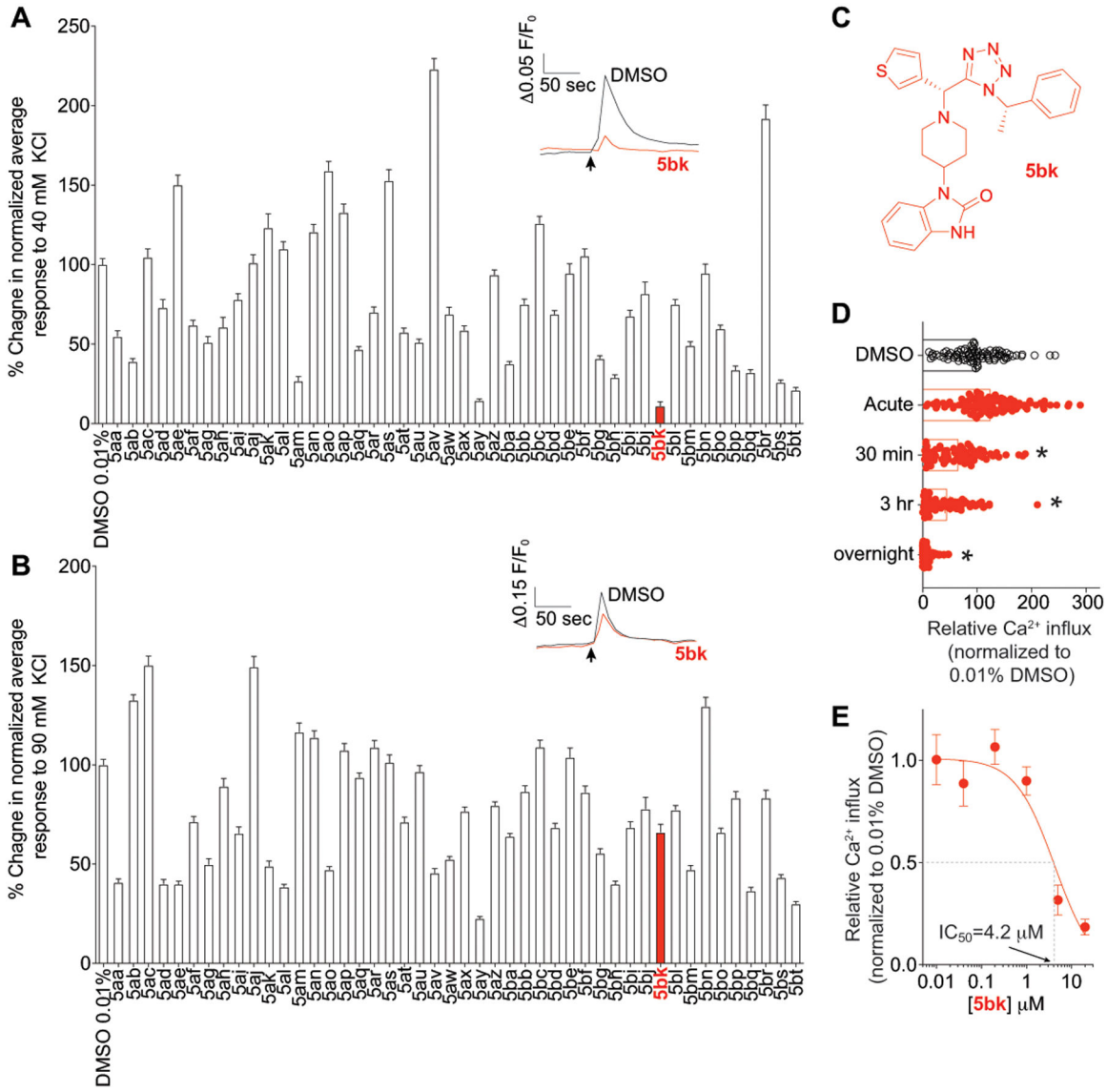

Figure 1. Primary screening using depolarization evoked Ca^{2+} influx in DRG neurons identifies several regulators of low and high voltage-activated calcium channels.

Peak calcium responses of sensory neurons incubated overnight with 20μM of the indicated compounds in response to 40 mM KCl (**A**) or 90 mM KCl (**B**) and normalized to 0.01% DMSO-treated control. N >78 neurons per condition from at least 3–4 rats each. Representative time courses of the change in 340 nm/380 nm ratio for the response of 4 representative neurons imaged in a preparation treated with 0.01% DMSO or **5bk**. Because an increase in intracellular calcium induces an increase in 340-nm emission and a decrease in 380-nm emission, the simultaneous increase in 340 nm and decrease in 380-nm fluorescence emission associated with application of KCl is indicative an increase in intracellular calcium. KCl was added at the time indicated by the arrow. (**C**) The structure of **5bk** is shown. (**D**) Scatter bar graph shows peak calcium responses of sensory neurons in response to a 40 mM KCl challenge. Neurons were incubated with vehicle (0.01% DMSO) or a 20μM concentration of **5bk** for various period of time as indicated: acutely (less than 5

min), 30 min, 2 hours, or 12–18 hours (overnight). (**E**) Concentration response curve for **5bk** inhibition of calcium influx in response to a 40 mM KCl challenge; neurons were treated with vehicle (0.01% DMSO) or a 20μM concentration of **5bk** overnight in this experiment. P values of comparisons between treatments are as indicated; see statistical analysis described in Table 1.

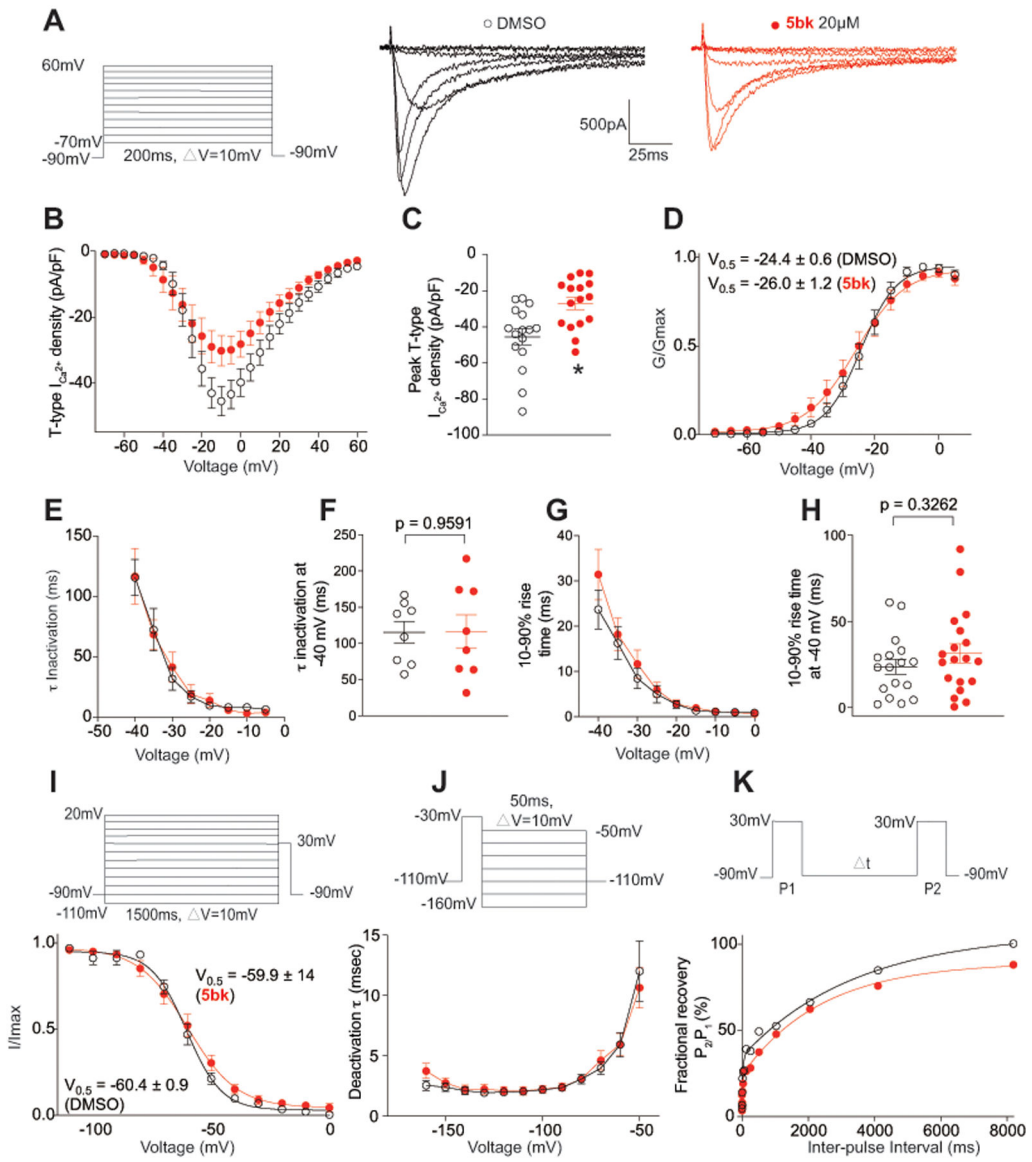

Figure 2. 5bk decreases T-Type Ca^{2+} currents in dorsal root ganglion (DRG) sensory neurons.

(**A**) Representative family of traces of T-Type Ca^{2+} currents from DRG sensory treated overnight with vehicle (0.01% DMSO) or **5bk** (20 μM). Voltage protocol used to evoke the currents is shown. (**B**) Summary of the normalized (pA/pF) T-Type calcium current density versus voltage relationship and (**C**) peak T-Type Ca^{2+} current density at −10 mV (mean ± SEM) from DRG sensory neurons treated as indicated. (**D**) Boltzmann fits for normalized conductance G/G_{max} voltage relations for voltage dependent activation of T-type currents. (**E**) Inactivation **τ**, which is calculated from a single-exponential fit of the decaying portion of the current waveforms using a single-exponential equation: $y = A_1 \times e^{(-x/\tau 1)} + y_0$, where A_1 is the amplitude, τ_1 is the decay constant, and y_0 is the offset. (**F**) This analysis was also isolated at −40 mV. (**G**) Time-dependent activation (10–90% rise time) from I-V curves and at −40mV (**H**) in DRG cells shown calculated from the data in **B**. (**I**) Boltzmann fits for normalized conductance G/G_{max} voltage relations for voltage dependent inactivation of

sensory neurons treated as indicated. (**J**) Deactivating tail currents in DRG neurons treated with vehicle (0.01% DMSO) or **5bk** (20 μM) were fit with a single-exponential function. The resulting **τ** values are plotted. (**K**) Recovery from inactivation in indicated groups. Data are averaged and fitted by double exponential association (n=16–19 cells per condition). All graphs show mean ± s.e.m. with individual data points showed when possible. P values of comparisons between treatments are as indicated; see statistical analysis described in Table 1.

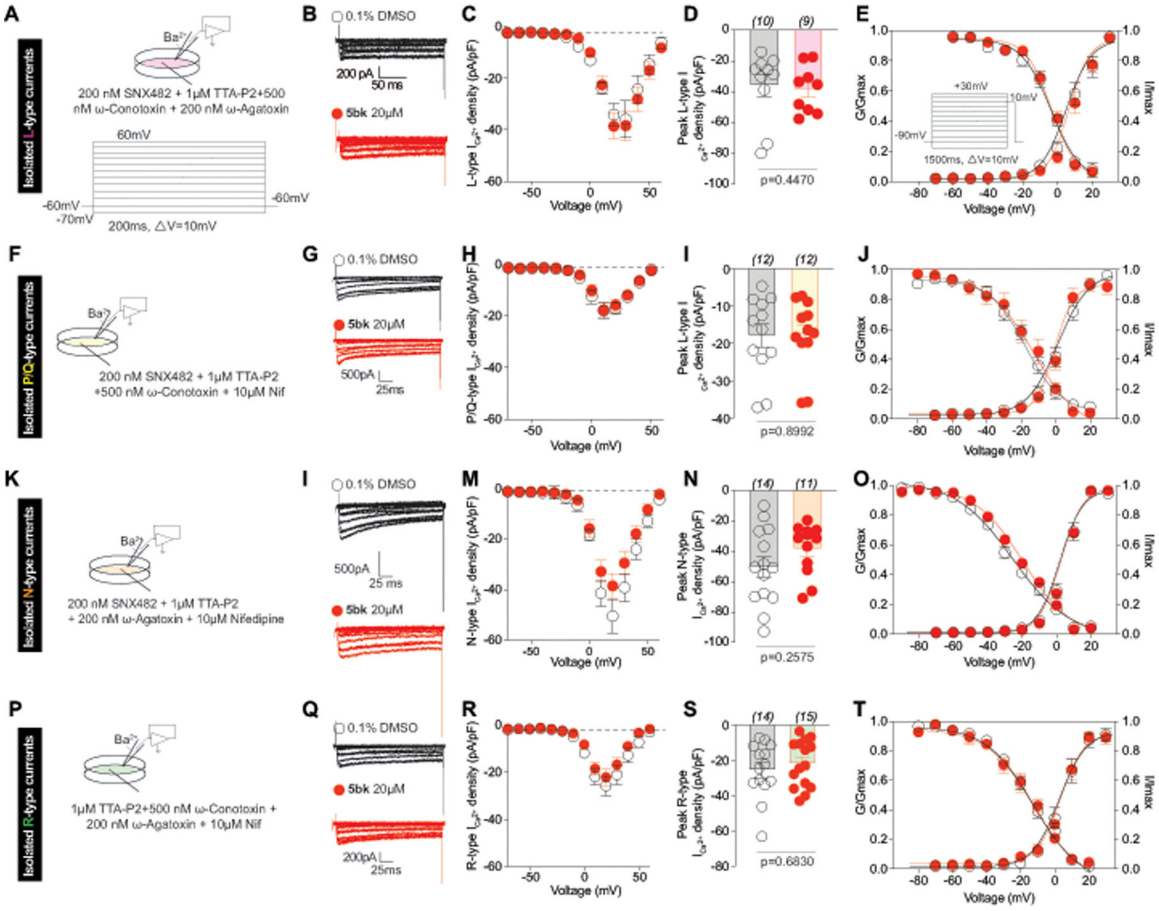

Figure 3. 5bk does not inhibit high voltage-activated Ca^{2+} currents in dorsal root ganglion (DRG) sensory neurons.

(**A**, **F**, **K**, **P**) Pharmacological isolation was achieved by the indicated cocktail of toxins/ small molecules. The voltage protocol used to elicit the currents is also shown. (**B**, **G**, **I**, **Q**) Representative traces of DRG neurons treated overnight with 0.1% DMSO (control) or 20 μM **5bk**. (**C**, **H**, **M, R**) Summary of the normalized (pA/pF) HVA calcium current density versus voltage relationship and (**D**, **I**, **N**, **S**) peak HVA Ca^{2+} current density at +20 mV (mean ± SEM) from DRG sensory neurons treated as indicated. Boltzmann fits for normalized conductance G/G_{max} voltage relations for voltage dependent activation and inactivation (**E, J**, **O**, **T**) of sensory neurons treated as indicated. Voltage dependent activation was assessed with the protocol shown in (**E**). The $V_{0.5}$ and slope (*k*) values for activation and inactivation are presented in Supplementary Figure 5. P values of comparisons between treatments are as indicated; see statistical analysis described in Table 1.

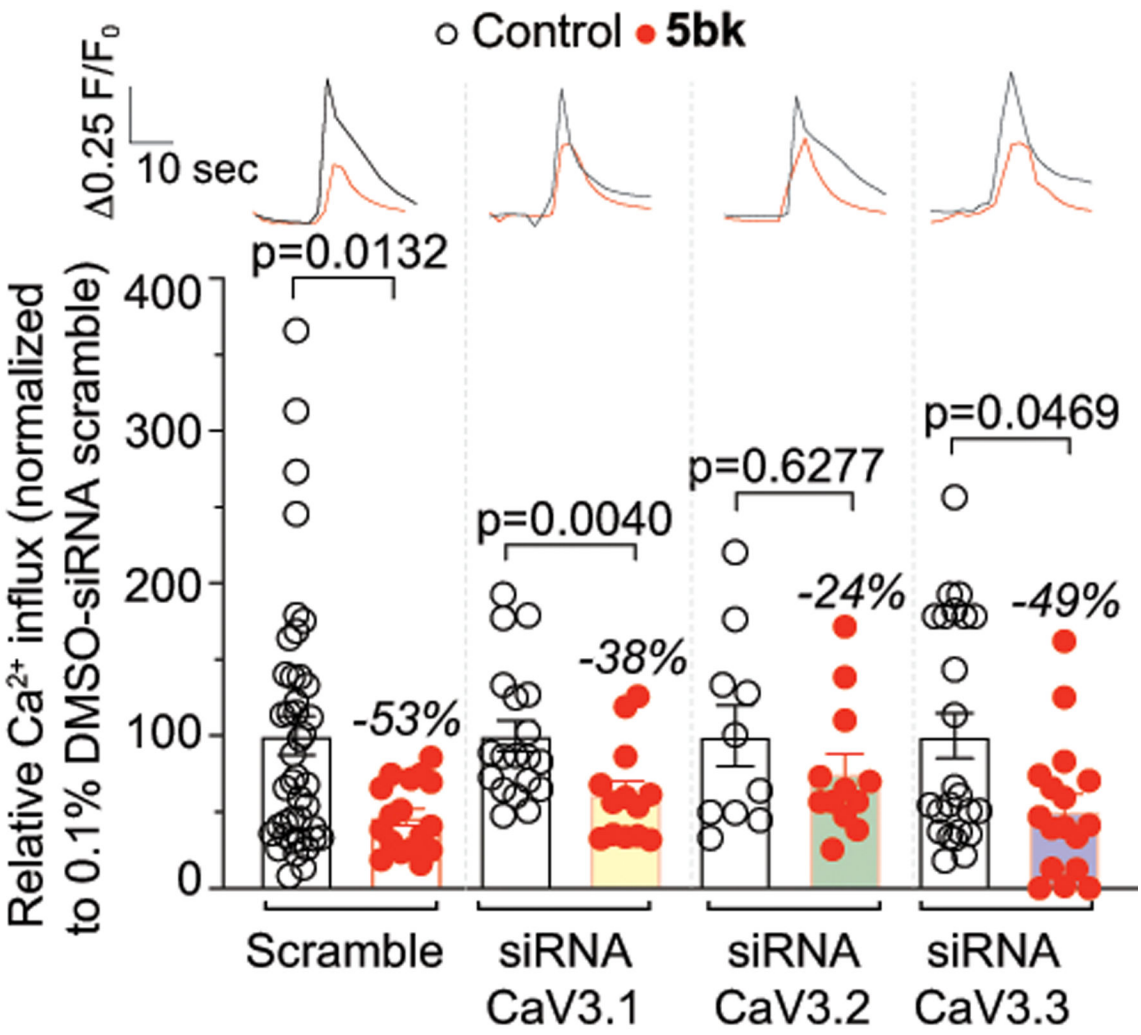

Figure 4. Downregulation of CaV3.2 blocks 5bk-mediated regulation of depolarization-evoked Ca^2 influx through T-type Ca^{2+} channels.

Dorsal root ganglion neurons were transfected during plating with a GFP construct and a scramble siRNA or with siRNAs against CaV3.1, CaV3.2 or CaV3.3. The bar graph shows normalized peak calcium response averages ± S.E.M. of DRG sensory neurons treated as indicated. Responses were normalized to that of DMSO (vehicle) in the siRNA scramble condition. Representative time courses of the change in 340 nm/380 nm ratio for the response of representative neurons imaged in a preparation treated with 0.01% DMSO or **5bk** are shown above the bar graphs. These experiments were done in a blinded fashion. P values of comparisons between treatments (n = 10–42 cells per condition) are as indicated; see statistical analysis described in Table 1.

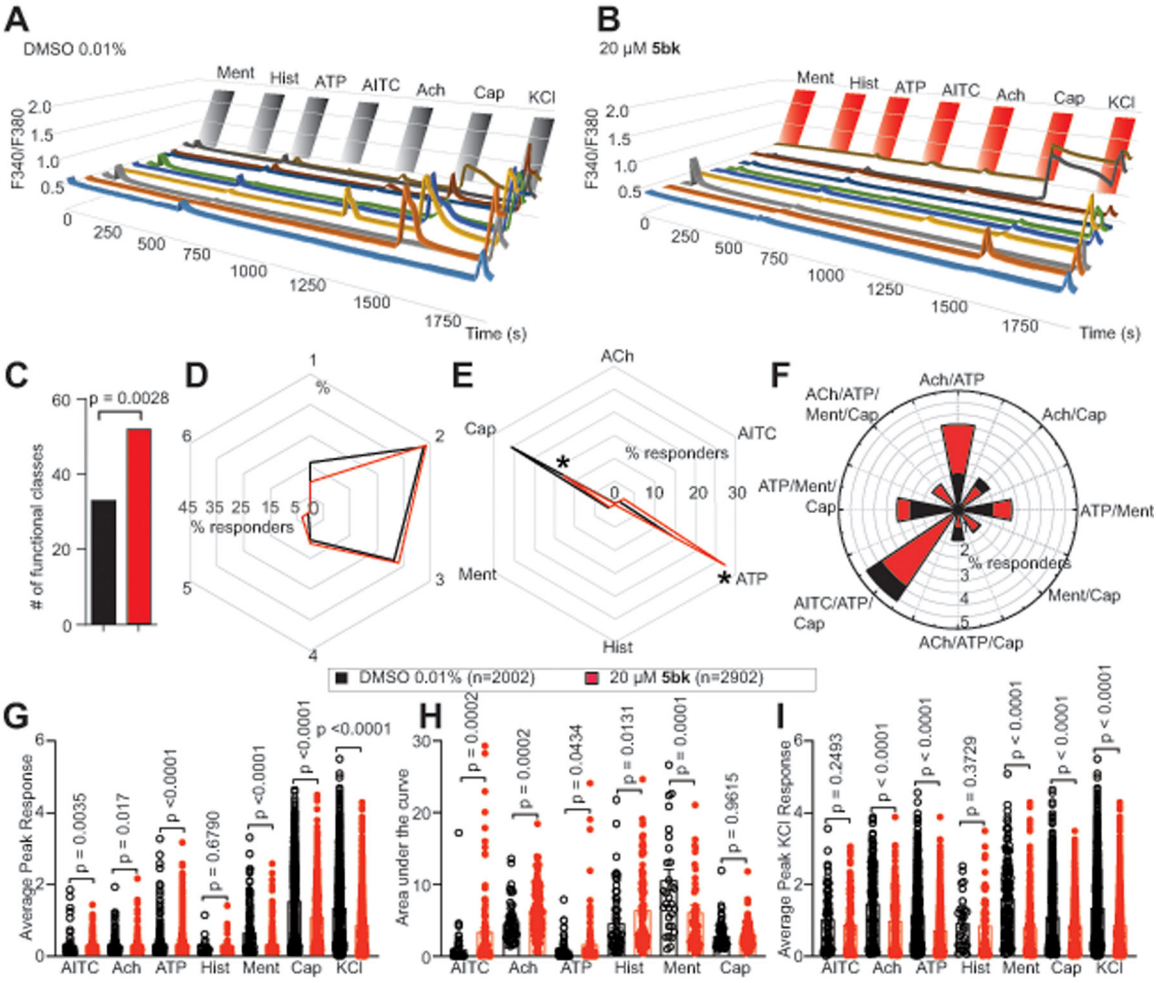

Figure 5. Constellation pharmacology-based characterization of neuronal populations in DRG sensory neurons treated with 5bk.

(**A**) Representative traces of sensory neurons treated overnight with 0.01% DMSO (vehicle) or (**B**) 20 μM concentration of **5bk** responding to constellation pharmacology triggers (menthol (400 nM), histamine (50 μM), ATP (10 μM), AITC (200 μM), acetylcholine (1 mM), capsaicin (100 nM) and KCl (90 mM)) during Ca^{2+} imaging. Each trace represents an individual neuron; a typical experimental trial records the responses of >300 neurons concurrently. (**C**) Number of overall functional DRG sensory neuronal classes as a result of treatment with DMSO or **5bk** (20 μM). (**D**) Percentage of DRG sensory neurons that responded to indicated number of triggers. (**E**) Percentage of sensory neurons responding to major classes and (**F**) indicated subclasses of constellation triggers. (**G**) Average peak Ca^{2+} response post-indicated treatment for DRG neurons following stimulation by major classes of constellation triggers. (**H**) Area under the curve is shown for calcium response in sensory neurons post-indicated treatment, after stimulation by major classes of constellation triggers. Area under the curve was calculated with Graphpad Prism software using the trapezoid rule. (**I**) Average peak KCl-evoked response of sensory neurons post-indicated treatment. P values of comparisons between treatments are as indicated; see statistical analysis described in Table 1. Abbreviations for constellation triggers are as follows: ACh = acetylcholine; AITC

= allyl isothiocyanate; ATP = adenosine triphosphate; Hist = histamine; Ment = menthol; Cap = capsaicin; KCl = potassium chloride. Data was collected from a total of 5 independent experiments with an overall sample of 2002 for control conditions and 2902 for **5bk** (20 μM). P values of comparisons between treatments are as indicated; see statistical analysis described in Table 1.

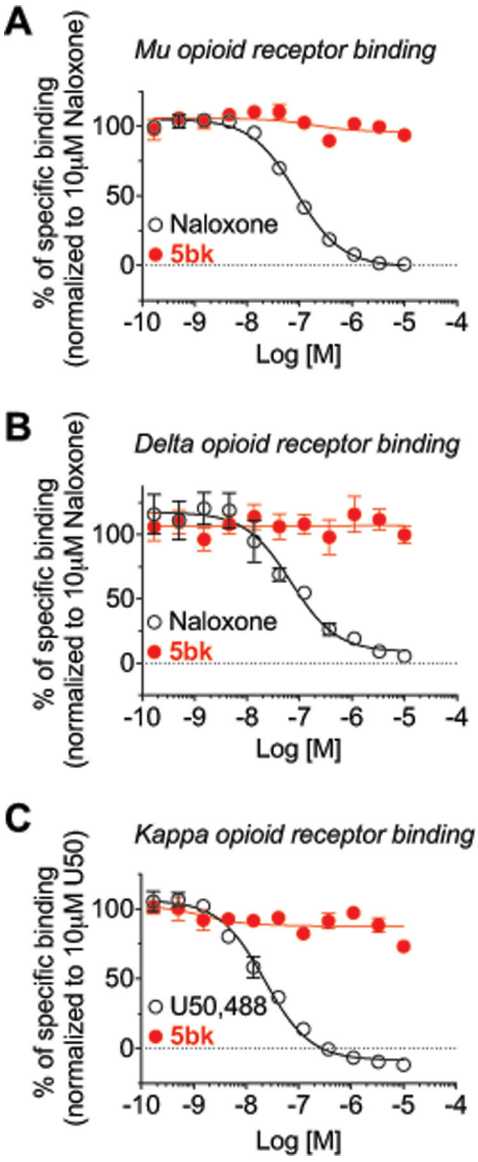

Figure 6. 5bk does not bind to the opioid receptors.

Competition radioligand binding was performed in CHO cells expressing the human mu/delta/kappa opioid receptors (MOR, DOR, or KOR, respectively) (see Methods for details). **5bk** or a positive control compound was competed against ^{3}H-diprenorphine in all 3 cell lines. Curves reported as the mean ± SEM of the mean value from each individual experiment in n = 3 independent experiments. The Ki also reported as the mean ± SEM of the individual value from each of n = 3 independent experiments. **5bk** did not produce competition binding up to 10 μM in any cell line. **(A)** MOR: Naloxone Ki = 43.3 ± 1.9 nM. **(B)** DOR: Naloxone Ki = 48.1 ± 9.1 nM. **(C)** KOR: U50,488 Ki = 12.7 ± 0.6 nM. See statistical analysis described in Table 1.

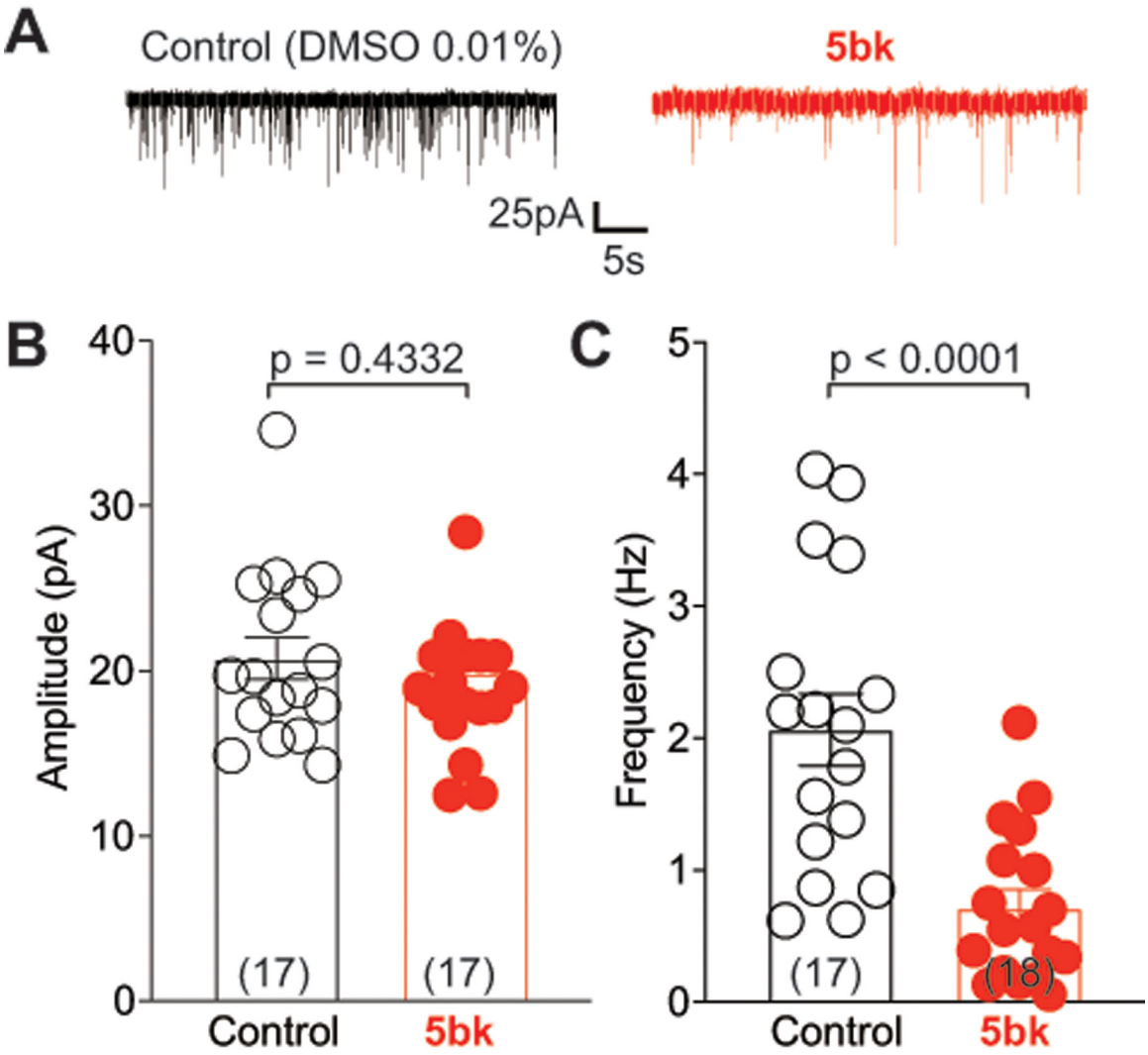

Figure 7. 5bk decreases spontaneous excitatory synaptic transmission in *substantia gelatinosa* neurons.

(A) Representative traces recorded from control (0.1% DMSO) and **5bk** (25 μM)-treated groups. (**B**) Spontaneous excitatory post synaptic current (EPSC) amplitudes as a result of treatment with DMSO or **5bk**. (**C**) Spontaneous EPSC frequency as a result of treatment with DMSO or **5bk**. P values of comparisons between treatments (n = 17–18 per condition) are as indicated; see statistical analysis described in Table 1.

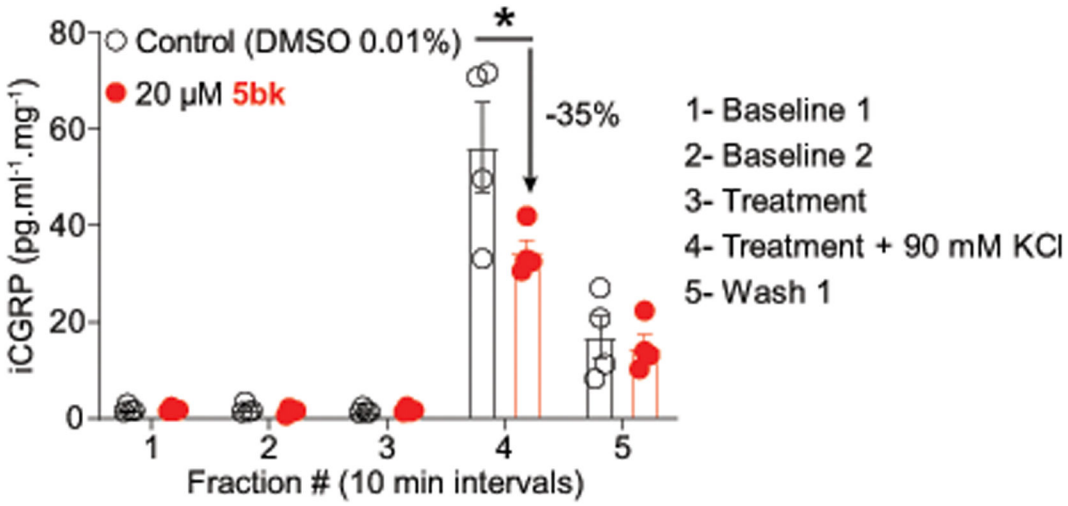

Figure 8. 5bk decreases evoked CGRP release.

Spinal cords from adult rats (n=4 per condition) were used to assess potassium chloride (KCl, 90 mM)-induced calcitonin gene related peptide (CGRP) release from nerve terminals. KCl increased CGRP release in control rat spinal cords, which was significantly higher than in cords from **5bk**-treated rats (* $p<0.05$ vs. control; two-way ANOVA *post hoc* Sidak's test). P values of comparisons between treatments are as indicated; see statistical analysis described in Table 1.

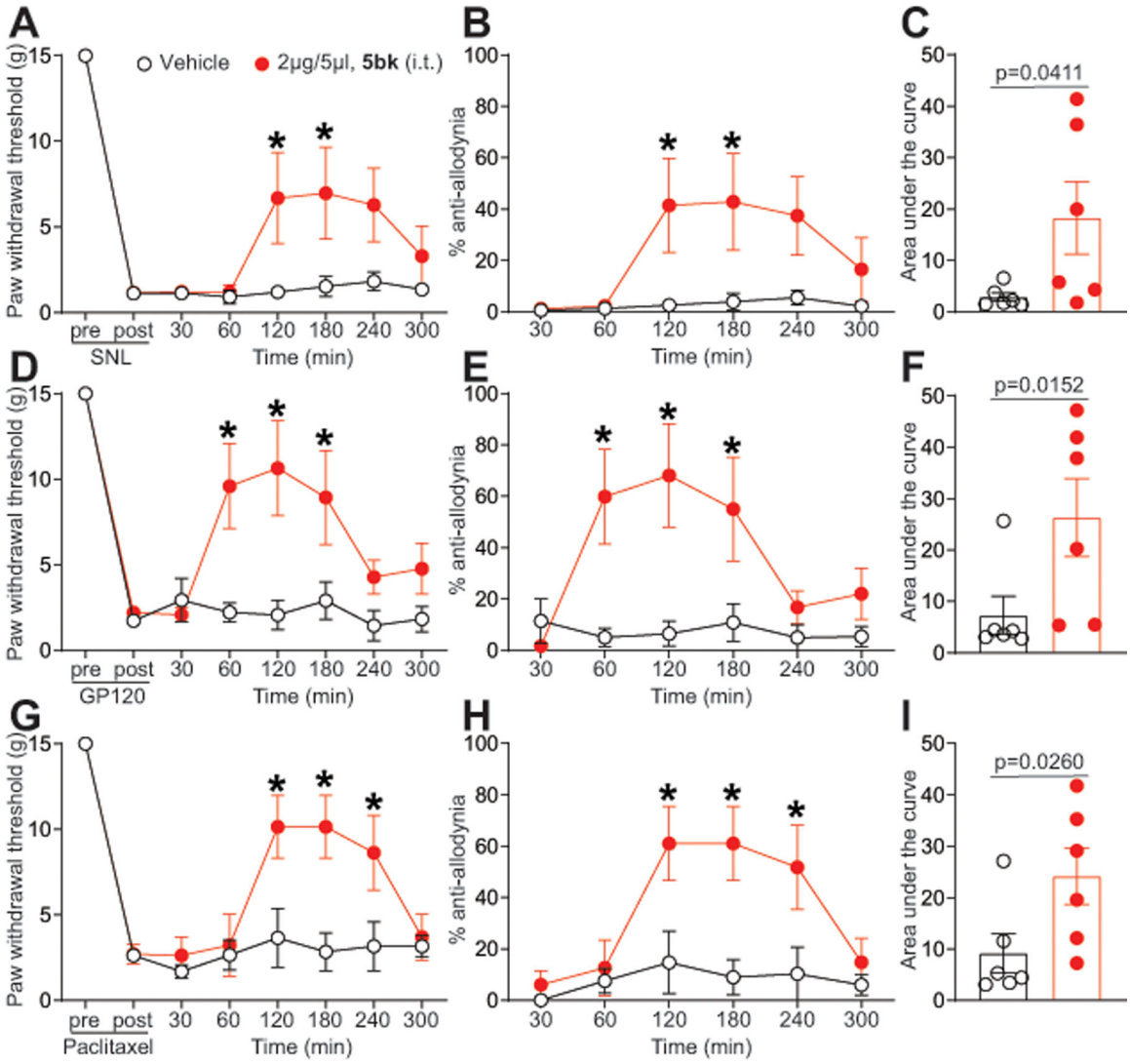

Figure 9. GP120, paclitaxel, and spinal nerve ligation induced nociceptive behaviors are reduced upon treatment with 5bk.

(**A**) Rats received spinal nerve ligation (SNL) injury with allodynia measurement on the left hind paw. Paw withdrawal thresholds were significantly decreased 7 days after surgery. **5bk** (2 µg/5 µL) or vehicle (saline) were injected into the intrathecal space and PWTs measured. Paw withdrawal thresholds were significantly reversed at the indicated times after injection of **5bk** (n=6; *p<0.05; two-way ANOVA with a Student-Neuman-Kuels post hoc test). (**B**) Data from D are transformed and presented as mean ± s.e.m. percentage of maximal anti-allodynia (see Methods). (**C**) Area under the curve (AUC), using the trapezoid method, for PWT. Statistical significance is indicated by asterisks (*p<0.05, one-way analysis of variance with Tukey's post hoc analysis) in comparison to vehicle-treated rats. (**D**) Paw withdrawal threshold (PWTs) of adult rats (n=7) was measured 15 days after 3 intrathecal injections of glycoprotein-120. Rats were treated with saline (vehicle) or **5bk** (2 µg/5 µL, intrathecal) as indicated. Asterisks indicate statistical significance compared with animals treated with saline (*p<0.05; 2-way ANOVA with a Dunnet's hoc test). (**E**) Data from A are

transformed and presented as mean ± s.e.m. percentage of maximal anti-allodynia (see Methods). (**F**) Area under the curve was derived as indicated before using Graphpad prism. Statistical significance is indicated by asterisks (*p<0.05, Mann-Whitney) in comparison to vehicle-treated rats. (**G**) Paw withdrawal threshold of adult rats (n=7) was measured 15 days after 4 intraperitoneal injections of paclitaxel. Rats were treated with saline (vehicle) or **5bk** (2 μg/5 μL, intrathecal) as indicated. Data from G are transformed and presented as mean ± s.e.m. percentage of maximal anti-allodynia (see Methods). Asterisks indicate statistical significance compared with tissue treated with saline (*p<0.05; 2-way ANOVA with a Dunnet's post hoc test). (**I**) Area under the curve was derived again as indicated before using Graphpad prism. Statistical significance is indicated by asterisks (*p<0.05, Mann-Whitney) in comparison to vehicle-treated rats. Exact p values of comparisons between treatments are described in Table 1.

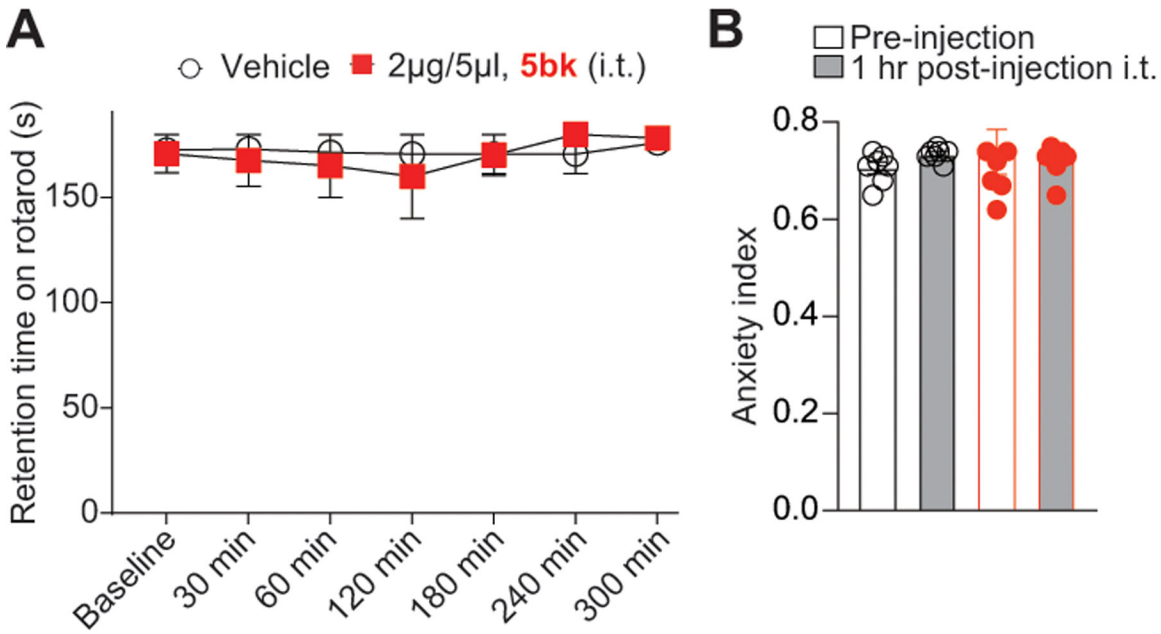

Figure 10. Treatment with 5bk does not induce motor deficits or alter anxiety levels.

(**A**) Rats (n = 6) were subjected to the rotarod performance test as previously described in the Methods in order to test for motor deficits. Vehicle and **5bk**-treated animals remained on the rotarod for an average of 172 ± 7.3 and 170 ± 9.6 seconds (cutoff 180 seconds), respectively, when tested over the course of 300 minutes. No significant motor deficits were noted in comparison to vehicle-treated animals. (**B**) Rats (n = 7) were subjected to the elevated plus maze (EPM) test as detailed (see methods); the anxiety index, integrates measurement of times and entries of the animals into the open and closed arms of the EPM, and is shown both pre- and post (1 hour) injection of either 0.01% DMSO (vehicle) or **5bk** (2 µg/5 µL, intrathecal) as indicated. See statistical analysis described in Table 1.

Table 1.

Statistical analyses of experiments.

Figure panel	Assay	Statistical test; findings	Post-hoc analysis (adjusted p-values)	Number of subjects	Number of subjects excluded (ROUT test)
Figure 1A	Calcium imaging – screening with a 40 mM KCl challenge	One-way ANOVA p <0.0001	Dunnett's multiple comparisons test DMSO 0.01% vs. 5aa <0.0001 DMSO 0.01% vs. 5ab <0.0001 DMSO 0.01% vs. 5ac 0.9988 DMSO 0.01% vs. 5ad 0.0023 DMSO 0.01% vs. 5ae <0.0001 DMSO 0.01% vs. 5af <0.0001 DMSO 0.01% vs. 5ag <0.0001 DMSO 0.01% vs. 5ah <0.0001 DMSO 0.01% vs. 5ai <0.0001 DMSO 0.01% vs. 5aj 0.9998 DMSO 0.01% vs. 5ak 0.014 DMSO 0.01% vs. 5al 0.5522 DMSO 0.01% vs. 5am <0.0001 DMSO 0.01% vs. 5an 0.0012 DMSO 0.01% vs. 5ao <0.0001 DMSO 0.01% vs. 5ap <0.0001 DMSO 0.01% vs. 5aq <0.0001 DMSO 0.01% vs. 5ar <0.0001 DMSO 0.01% vs. 5as <0.0001 DMSO 0.01% vs. 5at <0.0001 DMSO 0.01% vs. 5au <0.0001 DMSO 0.01% vs. 5av <0.0001 DMSO 0.01% vs. 5aw <0.0001 DMSO 0.01% vs. 5ax <0.0001 DMSO 0.01% vs. 5ay <0.0001 DMSO 0.01% vs. 5az 0.9264 DMSO 0.01% vs. 5ba <0.0001 DMSO 0.01% vs. 5bb <0.0001 DMSO 0.01% vs. 5bc <0.0001 DMSO 0.01% vs. 5bd <0.0001 DMSO 0.01% vs. 5be 0.9987 DMSO 0.01% vs. 5bf 0.9988 DMSO 0.01% vs. 5bg <0.0001 DMSO 0.01% vs. 5bh <0.0001 DMSO 0.01% vs. 5bi <0.0001 DMSO 0.01% vs. 5bj 0.767 DMSO 0.01% vs. 5bk <0.0001 DMSO 0.01% vs. 5bl <0.0001 DMSO 0.01% vs. 5bm <0.0001	DMSO 0.01% n= 1032 5aa n= 378 5ab n= 995 5ac n= 471 5ad n= 200 5ae n= 554 5af n= 244 5ag n= 242 5ah n= 275 5ai n= 542 5aj n= 409 5ak n= 214 5al n= 590 5am n= 216 5an n= 437 5ao n= 567 5ap n= 222 5aq n= 683 5ar n= 455 5as n= 357 5at n= 934 5au n= 885 5av n= 534 5aw n= 264 5ax n= 597 5ay n= 852 5az n= 1132 5ba n= 802 5bb n= 567 5bc n= 530 5bd n= 751 5be n= 348 5bf n= 284 5bg n= 747 5bh n= 802 5bi n= 644 5bj n= 95 5bk n= 78 5bl n= 958 5bm n= 381 5bn n= 100 5bo n= 559 5bp n= 604 5bq n= 681 5br n= 543 5bs n= 1250 5bt n= 914	

Figure panel	Assay	Statistical test; findings	Post-hoc analysis (adjusted p-values)	Number of subjects	Number of subjects excluded (ROUT test)
			DMSO 0.01% vs. 5bn 0.9994 DMSO 0.01% vs. 5bo <0.0001 DMSO 0.01% vs. 5bp <0.0001 DMSO 0.01% vs. 5bq <0.0001 DMSO 0.01% vs. 5br <0.0001 DMSO 0.01% vs. 5bs <0.0001 DMSO 0.01% vs. 5bt <0.0001		
Figure 1B	Calcium imaging - screening with a 90 mM KCl challenge	One-way ANOVA p <0.0001	Dunnett's multiple comparisons test DMSO 0.01% vs. 5aa <0.0001 DMSO 0.01% vs. 5ab <0.0001 DMSO 0.01% vs. 5ac <0.0001 DMSO 0.01% vs. 5ad <0.0001 DMSO 0.01% vs. 5ae <0.0001 DMSO 0.01% vs. 5af <0.0001 DMSO 0.01% vs. 5ag <0.0001 DMSO 0.01% vs. 5ah 0.3379 DMSO 0.01% vs. 5ai <0.0001 DMSO 0.01% vs. 5aj <0.0001 DMSO 0.01% vs. 5ak <0.0001 DMSO 0.01% vs. 5al <0.0001 DMSO 0.01% vs. 5am 0.0086 DMSO 0.01% vs. 5an 0.0086 DMSO 0.01% vs. 5ao <0.0001 DMSO 0.01% vs. 5ap 0.9803 DMSO 0.01% vs. 5aq 0.7626 DMSO 0.01% vs. 5ar 0.3921 DMSO 0.01% vs. 5as 0.9997 DMSO 0.01% vs. 5at <0.0001 DMSO 0.01% vs. 5au 0.9984 DMSO 0.01% vs. 5av <0.0001 DMSO 0.01% vs. 5aw <0.0001 DMSO 0.01% vs. 5ax <0.0001 DMSO 0.01% vs. 5ay <0.0001 DMSO 0.01% vs. 5az <0.0001 DMSO 0.01% vs. 5ba <0.0001 DMSO 0.01% vs. 5bb 0.0046 DMSO 0.01% vs. 5bc 0.285 DMSO 0.01% vs. 5bd <0.0001 DMSO 0.01% vs. 5be 0.9988 DMSO 0.01% vs. 5bf 0.0577 DMSO 0.01% vs. 5bg <0.0001 DMSO 0.01% vs. 5bh <0.0001 DMSO	DMSO 0.01% n= 1032 5aa n= 378 5ab n= 995 5ac n= 471 5ad n= 200 5ae n= 554 5af n= 244 5ag n= 242 5ah n= 275 5ai n= 542 5aj n= 409 5ak n= 214 5al n= 590 5am n= 216 5an n= 437 5ao n= 567 5ap n= 222 5aq n= 683 5ar n= 455 5as n= 357 5at n= 934 5au n= 885 5av n= 534 5aw n= 264 5ax n= 597 5ay n= 852 5az n= 1132 5ba n= 802 5bb n= 567 5bc n= 530 5bd n= 751 5be n= 348 5bf n= 284 5bg n= 747 5bh n= 802 5bi n= 644 5bj n= 95 5bk n= 78 5bl n= 958 5bm n= 381 5bn n= 100 5bo n= 559 5bp n= 604 5bq n= 681 5br n= 543	

Figure panel	Assay	Statistical test; findings	Post-hoc analysis (adjusted p-values)	Number of subjects	Number of subjects excluded (ROUT test)
			0.01% vs. 5bi <0.0001 DMSO 0.01% vs. 5bj 0.0564 DMSO 0.01% vs. 5bk <0.0001 DMSO 0.01% vs. 5bl <0.0001 DMSO 0.01% vs. 5bm <0.0001 DMSO 0.01% vs. 5bn 0.0007 DMSO 0.01% vs. 5bo <0.0001 DMSO 0.01% vs. 5bp <0.0001 DMSO 0.01% vs. 5bq <0.0001 DMSO 0.01% vs. 5br <0.0001 DMSO 0.01% vs. 5bs <0.0001 DMSO 0.01% vs. 5bt <0.0001	5bs n= 1250 5bt n= 914	
Figure 1D	Calcium imaging – time course of effect of 5bk	One-way ANOVA p <0.0001	Dunnett's multiple comparisons test DMSO 0.01% vs. Acute p = 0.1863 DMSO 0.01% vs. 30 min p = 0.0043 DMSO 0.01% vs. 3 hr p < 0.0001 DMSO 0.01% vs. overnight p < 0.0001	DMSO 0.01% n = 87 Acute 5bk n = 108 30 min 5bk n = 81 3 hr 5bk n = 75 overnight 5 bk n= 128	
Figure 1E	Calcium imaging – concentration response of 5bk	Non-linear regression	[Iinhibitor] vs. response (three parameters) IC50 = 4.195 μM; r^2 = 0.4137		
Figure 2C	Whole cell patch clamp electrophysiology – Peak T type currents		Unpaired t-test DMSO 0.01% vs. 5bk 20 μM p =0.2343 ($V_{0.5}$) and p = 0.1009 (*k*)	DMSO 0.01% n = 16 5bk n = 16	
Figure 2D	Whole cell patch clamp electrophysiology – Voltage-dependence of half-activation ($V_{0.5}$) and slope (*k*)	Non-parametric test	Mann-Whitney test $V_{0.5}$: DMSO 0.01% vs. 5bk 20 μM p =0.0019	DMSO 0.01% n = 16 5bk n = 16	
Figure 2F	Whole cell patch clamp electrophysiology – $\tau_{inactivation}$		Mann-Whitney test DMSO 0.01% vs. 5bk 20 μM p =0.9591	DMSO 0.01% n = 8 5bk n = 8	
Figure 2H	Whole cell patch clamp electrophysiology – 0–90% rise time at −40 mV		Mann-Whitney test DMSO 0.01% vs. 5bk 20 μM p =0.3292	DMSO 0.01% n = 17 5bk n = 19	
Figure 2I	Whole cell patch clamp electrophysiology – Voltage-dependence of half-inactivation ($V_{0.5}$) and slope (*k*)		Unpaired t-test DMSO 0.01% vs. 5bk 20 μM p =0.7833 ($V_{0.5}$) and p = 0.0575 (*k*)	DMSO 0.01% n = 15 5bk n = 16	
Figure 3D	Whole cell patch clamp electrophysiology – Peak L type currents		Mann-Whitney test DMSO 0.01% vs. 5bk 20 μM p =0.4470	DMSO 0.01% n = 10 5bk n = 9	
Figure 3E	Whole cell patch clamp electrophysiology – Voltage-dependence of		Mann-Whitney test DMSO 0.01% vs. 5bk 20 μM	DMSO 0.01% n = 10 5bk n = 9	

Figure panel	Assay	Statistical test; findings	Post-hoc analysis (adjusted p-values)	Number of subjects	Number of subjects excluded (ROUT test)
	half-activation and inactivation ($V_{0.5}$) and slopes (*k*) of L-type currents		p =0.2222 (for Activation $V_{0.5}$) DMSO 0.01% vs. 5bk 20 μM p =0.9318 (for Activation *k*) DMSO 0.01% vs. 5bk 20 μM p =0.2222 (for Inactivation $V_{0.5}$) DMSO 0.01% vs. 5bk 20 μM p =0.4862 (for Inactivation *k*)		
Figure 3I	Whole cell patch clamp electrophysiology – Peak P/Q type currents		Mann-Whitney test DMSO 0.01% vs. 5bk 20 μM p =0.8992	DMSO 0.01% n = 12 5bk n = 12	
Figure 3J	Whole cell patch clamp electrophysiology – Voltage-dependence of half-activation and inactivation ($V_{0.5}$) and slopes (*k*) of P/Q-type currents		Mann-Whitney test DMSO 0.01% vs. 5bk 20 μM p =0.2496 (for Activation $V_{0.5}$) DMSO 0.01% vs. 5bk 20 μM p =0.0694 (for Activation *k*) DMSO 0.01% vs. 5bk 20 μM p =0.2017 (for Inactivation $V_{0.5}$) DMSO 0.01% vs. 5bk 20 μM p =0.3637 (for Inactivation *k*)	DMSO 0.01% n = 10 5bk n = 8	
Figure 3N	Whole cell patch clamp electrophysiology – Peak N type currents		Mann-Whitney test DMSO 0.01% vs. 5bk 20 μM p =0.2575	DMSO 0.01% n = 14 5bk n = 12	
Figure 3O	Whole cell patch clamp electrophysiology – Voltage-dependence of half-activation and inactivation ($V_{0.5}$) and slopes (*k*) of N-type currents		Mann-Whitney test DMSO 0.01% vs. 5bk 20 μM p =0.5003 (for Activation $V_{0.5}$) DMSO 0.01% vs. 5bk 20 μM p =0.8481 (for Activation *k*) DMSO 0.01% vs. 5bk 20 μM p =0.0930 (for Inactivation $V_{0.5}$) DMSO 0.01% vs. 5bk 20 μM p =0.2784 (for Inactivation *k*)	DMSO 0.01% n = 12 5bk n = 17	
Figure 3S	Whole cell patch clamp electrophysiology – Peak R type currents		Mann-Whitney test DMSO 0.01% vs. 5bk 20 μM p =0.6830	DMSO 0.01% n = 14 5bk n = 15	
Figure 3T	Whole cell patch clamp electrophysiology – Voltage-dependence of half-activation and inactivation ($V_{0.5}$) and slopes (*k*) of R type currents		Mann-Whitney test DMSO 0.01% vs. 5bk 20 μM p =0.7532 (for Activation $V_{0.5}$) DMSO 0.01% vs. 5bk 20 μM p =0.5951 (for Activation *k*) DMSO 0.01% vs. 5bk 20 μM p =0.9038 (for Inactivation $V_{0.5}$) DMSO 0.01% vs. 5bk 20		

Figure panel	Assay	Statistical test; findings	Post-hoc analysis (adjusted p-values)	Number of subjects	Number of subjects excluded (ROUT test)
			μM p =0.8727 (for Inactivation *k*)		
Figure 4	Calcium imaging	Non-parametric test	Mann-Whitney test Scramble DMSO vs. Scramble 5bk p = 0.0132 siRNA CaV3.1 DMSO vs. siRNA CaV3.1 5bk p = 0.0040 siRNA CaV3.2 DMSO vs. siRNA CaV3.2 5bk p = 0.6277 siRNA CaV3.3 DMSO vs. siRNA CaV3.3 5bk p = 0.0469	Scramble DMSO n = 42 Scramble 5bk n = 17 siRNA CaV3.1 DMSO n = 19 siRNA CaV3.1 5bk n = 13 siRNA CaV3.2 DMSO n = 10 siRNA CaV3.2 5bk n =12 siRNA CaV3.3 DMSO n = 24 siRNA CaV3.3 5bk n = 17	
Figure 5C	Constellation pharmacology - # of functional classes	z-test	DMSO 0.01% vs. 5bk 20 μM P=0.00288		
Figure 5D	Constellation pharmacology - % responders	z-test	DMSO 0.01% vs. 5bk 20 μM 1 response: p=0.02144 2 response: p=0.63122 3 response: p=0.48392 4 response: p=0.65994 5 response: p=0.60306 6 response: p=0.98404	DMSO 0.01% n=2002 cells 5bk 20 μM n=2902 cells	
Figure 5E	Constellation pharmacology - % responders	z-test	DMSO 0.01% vs. 5bk 20 μM AITC: p=0.41222 Acetylcholine: p=0.23404 ATP: p<0.00001 Histamine: p=0.77948 Menthol: p=0.10524 Capsaicin: p<0.00001	DMSO 0.01% n=2002 cells 5bk 20 μM n=2902 cells	
Figure 5F	Constellation pharmacology – average peak response	z-test	DMSO 0.01% vs. 5bk 20 μM ACh/ ATP: p=0.5552 ACh/ Cap: p=0.90448 ATP/ Menthol: p=0.79486 Menthol/ Cap: p=0.98404 AITC/ ATP/ Cap: p=0.86502 ACh/ ATP/ Cap: p=0.80258 ATP/ Menthol/ Cap: p=0.84148 AITC/ ATP/ Menthol/ Cap: p=0.8807	DMSO 0.01% n=2002 cells 5bk 20 μM n=2902 cells	
Figure 5G	P Constellation pharmacology – Peak response to trigger	Mann-Whitney	DMSO 0.01% vs. 5bk 20 μM AITC: p=0.017 Acetylcholine: p=0.0035 ATP: p<0.0001 Histamine: p=0.6790 Menthol: p<0.0001 Capsaicin: p<0.0001	DMSO 0.01% n=2002 cells 5bk 20 μM n=2902 cells	

Figure panel	Assay	Statistical test; findings	Post-hoc analysis (adjusted p-values)	Number of subjects	Number of subjects excluded (ROUT test)
			KCl: p<0.0001		
Figure 5H	Constellation pharmacology – area under the curve	Mann-Whitney	DMSO 0.01% vs. 5bk 20 μM AITC: p<0.0001 Acetylcholine: p=0.0002 ATP: p=0.0434 Histamine: p=0.0131 Menthol: p=0.0001 Capsaicin: p=0.9615	DMSO 0.01% n=2002 cells 5bk 20 μM n=2902 cells	
Figure 5I	Constellation pharmacology – Average Peak KCl response	Mann-Whitney	DMSO 0.01% vs. 5bk 20 μM AITC: p=0.2493 Acetylcholine: p<0.0001 ATP: p<0.0001 Histamine: p=0.3729 Menthol: p<0.0001 Capsaicin: p<0.0001 KCl: p<0.0001	DMSO 0.01% n=2002 cells 5bk 20 μM n=2902 cells	
Figure 6A–C	Competition Binding Assay for Mu, Delta, and Kappa opioid receptors	3 variable, 1 site binding non-linear regression curve-fit	5bk was reported as “Not Converged” for all 3 panels, meaning no measurable competition. Mathematically, this is defined as no fitted curve with an $R^2 > 0.6$.	Results in measure of affinity reported as mean Ki ± SEM of the N=3 set.	
Figure 7B	Slice electrophysiology – Amplitude of EPSCs	Mann-Whitney p = 0.4332		Control (DMSO 0.01%): n = 17 5bk (20 μM): n = 17	Control (DMSO 0.01%): n = 1 5bk (20 μM): n = 1
Figure 7C	Slice electrophysiology – Frequency of EPSCs	Mann-Whitney p < 0.0001		Control (DMSO 0.01%): n = 17 5bk (20 μM): n = 18	
Figure 8	CGRP release from spinal cords	Two-way ANOVA	Dunnett’s multiple comparisons test Baseline 1: DMSO 0.01% vs. 5bk 20 μM p =0.9998 Baseline 2: DMSO 0.01% vs. 5bk 20 μM p =0.9935 Treatment: DMSO 0.01% vs. 5bk 20 μM p =0.9994 Treatment plus 90 mM KCl: DMSO 0.01% vs. 5bk 20 μM p =0.0002 Wash: DMSO 0.01% vs. 5bk 20 μM p =0.8947	DMSO 0.01% n = 4 5bk n = 4 for all conditions	
Figure 9A	Spared nerve injury – paw withdrawal threshold	Two-way ANOVA	Sidak’s post hoc test Vehicle vs. 5 bk: Pre: p >0.9999 0 min: p >0.9999 30 min: p >0.9999 60 min: p >0.9999 120 min: p = 0.0150	Vehicle n = 6 5bk n = 6 for all conditions	

Figure panel	Assay	Statistical test; findings	Post-hoc analysis (adjusted p-values)	Number of subjects	Number of subjects excluded (ROUT test)
			180 min: p = 0.0162 240 min: p = 0.0828 300 min: p = 0.9074		
Figure 9B	Spared nerve injury – % anti-allodynia	Two-way ANOVA	Sidak's post hoc test Vehicle vs. 5 bk: 30 min: p >0.9999 60 min: p >0.9999 120 min: p = 0.0344 180 min: p = 0.0341 240 min: p = 0.1245 300 min: p = 0.8773	Vehicle n = 6 5bk n = 6 for all conditions	
Figure 9C	Spared nerve injury – Area under the curve		Mann Whitney test Vehicle vs. 5 bk p = 0.0411	Vehicle n = 6 5bk n = 6 for all conditions	
Figure 9D	GP120 – paw withdrawal threshold	Two-way ANOVA	Sidak's multiple comparisons post hoc test Vehicle vs. 5 bk: Pre: p >0.9999 0 min: p >0.9999 30 min: p = 0.9998 60 min: p = 0.0022 120 min: p = 0.0002 180 min: p = 0.0208 240 min: p = 0.7186 300 min: p = 0.6802	Vehicle n = 6 5bk n = 6 for all conditions	
Figure 9E	GP120 – % anti-allodynia	Two-way ANOVA	Sidak's multiple comparisons post hoc test Vehicle vs. 5 bk: 30 min: p = 0.9908 60 min: p = 0.0060 120 min: p = 0.0015 180 min: p = 0.0422 240 min: p = 0.9751 300 min: p = 0.8785	Vehicle n = 6 5bk n = 6 for all conditions	
Figure 9F	GP120 – Area under the curve		Mann Whitney test Vehicle vs. 5 bk p = 0.0152	Vehicle n = 6 5bk n = 6 for all conditions	
Figure 9G	Paclitaxel – paw withdrawal threshold	Two-way ANOVA	Sidak's multiple comparisons post hoc test Vehicle vs. 5 bk: Pre: p >0.9999 0 min: p >0.9999 30 min: p = 0.9994 60 min: p >0.9999 120 min: p = 0.0042 180 min: p = 0.0009 240 min: p = 0.0248 300 min: p >0.9999	Vehicle n = 6 5bk n = 6 for all conditions	

Figure panel	Assay	Statistical test; findings	Post-hoc analysis (adjusted p-values)	Number of subjects	Number of subjects excluded (ROUT test)
Figure 9H	Paclitaxel nerve injury – % anti-allodynia	Two-way ANOVA	Sidak's multiple comparisons post hoc test Vehicle vs. 5 bk: 30 min: p = 0.9989 60 min: p = 0.9996 120 min: p = 0.0134 180 min: p = 0.0040 240 min: p = 0.0346 300 min: p = 0.9912	Vehicle n = 6 5bk n = 6 for all conditions	
Figure 9I	Paclitaxel nerve injury – Area under the curve		Mann Whitney test Vehicle vs. 5 bk p = 0.0260	Vehicle n = 6 5bk n = 6	
Figure 10A	Rotarod	Two-way ANOVA	Sidak's multiple comparisons post hoc test Vehicle vs. 5 bk: Pre: p >0.9999 30 min: p = 0.9999 60 min: p = 0.9995 120 min: p = 0.9893 180 min: p >0.9999 240 min: p = 0.9960 300 min: p >0.9999	Vehicle n = 6 5bk n = 6 for all conditions	
Figure 10B	Anxiety (elevated plus maze)	Mann-Whitney p = 0.6230		Vehicle n = 7 5bk n = 7	